

KIEV TARAS SHEVCHENKO NATIONAL UNIVERSITY

RADIOPHYSICS FACULTY

Vladimirska St. 64,
252033 Kiev,
Ukraine

Tel: 380-44-220-8491

Fax: 380-44-224-6166

THE FINAL REPORT

ON THE SPECIAL CONTRACT SPC-97-4025

The Study of the Phase Characteristics of Bragg Cells for Acousto-Optic Signal
Processing

Principal investigator

A handwritten signature in black ink, appearing to be 'A. V. Yurchenko', written over a vertical line.

Mr. A. V. Yurchenko

REPORT DOCUMENTATION PAGE			Form Approved OMB No. 0704-0188		
Public reporting burden for this collection of information is estimated to average 1 hour per response, including the time for reviewing instructions, searching existing data sources, gathering and maintaining the data needed, and completing and reviewing this collection of information. Send comments regarding this burden estimate or any other aspect of this collection of information, including suggestions for reducing this burden to Department of Defense, Washington Headquarters Services, Directorate for Information Operations and Reports (0704-0188), 1215 Jefferson Davis Highway, Suite 1204, Arlington, VA 22202-4302. Respondents should be aware that notwithstanding any other provision of law, no person shall be subject to any penalty for failing to comply with a collection of information if it does not display a currently valid OMB control number. PLEASE DO NOT RETURN YOUR FORM TO THE ABOVE ADDRESS.					
1. REPORT DATE (DD-MM-YYYY) 01-01-1998		2. REPORT TYPE Final		3. DATES COVERED (FROM - TO) xx-xx-1998 to xx-xx-1998	
4. TITLE AND SUBTITLE The Study of the Phase Characteristics of Bragg Cells for Acousto-Optic Signal Processing Unclassified			5a. CONTRACT NUMBER F6170897W0095		
			5b. GRANT NUMBER		
			5c. PROGRAM ELEMENT NUMBER		
6. AUTHOR(S) Yurchenko, Alexander ;			5d. PROJECT NUMBER		
			5e. TASK NUMBER		
			5f. WORK UNIT NUMBER		
7. PERFORMING ORGANIZATION NAME AND ADDRESS Kiev Taras Shevchenko National University Vladimirskaya St. 64 Kiev 252033, Ukrainexxxxx			8. PERFORMING ORGANIZATION REPORT NUMBER		
9. SPONSORING/MONITORING AGENCY NAME AND ADDRESS EOARD PSC 802 BOX 14 FPO, 09499-0200			10. SPONSOR/MONITOR'S ACRONYM(S)		
			11. SPONSOR/MONITOR'S REPORT NUMBER(S)		
12. DISTRIBUTION/AVAILABILITY STATEMENT APUBLIC RELEASE					
13. SUPPLEMENTARY NOTES					
14. ABSTRACT This report results from a contract tasking Kiev Taras Shevchenko National University as follows: The contractor will determine the relationship of phase characteristics between TeO2 and GaAs cells with their constructive and technical parameters. Design a Braggcell TeO2 with minimal phase distortions operating near 100 MHz. Experimentally investigate the phase characteristics for a Bragg cell on TeO2. Thus, the basic results of the work are as follows: 1. A Bragg cell in a heterodyne (coherent) signal processing system does not insert any appreciable phase distortions into an output signal unless a photodetector size is less than a light spot one. 2. Otherwise, such distortions can offer and be appreciable causing an unavoidable frequency dependent phase noise and a dynamic range reduction. 3. In testing optical systems a Bragg cell wave-front distortions can cause a deterioration of system parameters. From the aforesaid follows that further experimental investigations using a photodiode array are useful and necessary to learn vividly real limitations of considered opto-electronic system application.					
15. SUBJECT TERMS EOARD; Electronic Devices; Optical Components; Signal Processing					
16. SECURITY CLASSIFICATION OF:		17. LIMITATION OF ABSTRACT Public Release	18. NUMBER OF PAGES 35	19. NAME OF RESPONSIBLE PERSON Fenster, Lynn lfenster@dtic.mil	
a. REPORT Unclassified	b. ABSTRACT Unclassified	c. THIS PAGE Unclassified		19b. TELEPHONE NUMBER International Area Code Area Code Telephone Number 703767-9007 DSN 427-9007	
				Standard Form 298 (Rev. 8-98) Prescribed by ANSI Std Z39.18	

REPORT DOCUMENTATION PAGE			Form Approved OMB No. 0704-0188	
Public reporting burden for this collection of information is estimated to average 1 hour per response, including the time for reviewing instructions, searching existing data sources, gathering and maintaining the data needed, and completing and reviewing the collection of information. Send comments regarding this burden estimate or any other aspect of this collection of information, including suggestions for reducing this burden to Washington Headquarters Services, Directorate for Information Operations and Reports, 1215 Jefferson Davis Highway, Suite 1204, Arlington, VA 22202-4302, and to the Office of Management and Budget, Paperwork Reduction Project (0704-0188), Washington, DC 20503.				
1. AGENCY USE ONLY (Leave blank)		2. REPORT DATE 1998		3. REPORT TYPE AND DATES COVERED Final Report
4. TITLE AND SUBTITLE The Study of the Phase Characteristics of Bragg Cells for Acousto-Optic Signal Processing			5. FUNDING NUMBERS F6170897W0095	
6. AUTHOR(S) Dr. Alexander Yurchenko				
7. PERFORMING ORGANIZATION NAME(S) AND ADDRESS(ES) Kiev Taras Shevchenko National University Vladimirska St. 64 Kiev 252033 Ukraine			8. PERFORMING ORGANIZATION REPORT NUMBER N/A	
9. SPONSORING/MONITORING AGENCY NAME(S) AND ADDRESS(ES) EOARD PSC 802 BOX 14 FPO 09499-0200			10. SPONSORING/MONITORING AGENCY REPORT NUMBER SPC 97-4025	
11. SUPPLEMENTARY NOTES				
12a. DISTRIBUTION/AVAILABILITY STATEMENT Approved for public release; distribution is unlimited.			12b. DISTRIBUTION CODE A	
13. ABSTRACT (Maximum 200 words) This report results from a contract tasking Kiev Taras Shevchenko National University as follows: The contractor will determine the relationship of phase characteristics between TeO2 and GaAs cells with their constructive and technical parameters. Design a Braggcell TeO2 with minimal phase distortions operating near 100 MHz. Experimentally investigate the phase characteristics for a Bragg cell on TeO2. Thus, the basic results of the work are as follows: 1. A Bragg cell in a heterodyne (coherent) signal processing system does not insert any appreciable phase distortions into an output signal unless a photodetector size is less than a light spot one. 2. Otherwise, such distortions can offer and be appreciable causing an unavoidable frequency dependent phase noise and a dynamic range reduction. 3. In testing optical systems a Bragg cell wave-front distortions can cause a deterioration of system parameters. From the aforesaid follows that further experimental investigations using a photodiode array are useful and necessary to learn vividly real limitations of considered opto-electronic system application.				
14. SUBJECT TERMS EOARD, Electronic Devices, Optical Components, Signal Processing			15. NUMBER OF PAGES 33	
			16. PRICE CODE N/A	
17. SECURITY CLASSIFICATION OF REPORT UNCLASSIFIED	18. SECURITY CLASSIFICATION OF THIS PAGE UNCLASSIFIED	19. SECURITY CLASSIFICATION OF ABSTRACT UNCLASSIFIED	20. LIMITATION OF ABSTRACT UL	

Kiev, 1998

AUTHORS:

A.V. Yurchenko, principle investigator;

V.A. Goncharov, sections 2, 4.2.1, 4.2.2,b;

L.N. Ilchenko, section 4.2;

V.M. Moskalev, section 4.1;

E.N. Smirnov, sections 3.4, 4.2;

G.F. Pogorelova, section 4.2.2,b;

V.P. Danko, V.N. Kurashov, D.V. Podanchuk, section 4.3.

CONTENTS

	page
1. Introduction	3
2. Calculation of an output phase of a photodetector (basic results of the first stage report)	5
3. Designing of a Bragg cell with small phase distortions	9
3.1 Common considerations	9
3.2 Designing of a Bragg cell for a given efficiency	10
3.3 Designing of a Bragg cell on TeO ₂ with operating frequency $f_0=100$ MHz	12
3.4 Designing of a Bragg cell on GaAS	13
4. Experiment	15
4.1 An experimental specimen	15
4.2 Measurement of phase response $\varphi(f)$ of the equivalent opto-electronic quadripole	15
4.2.1 Conventional technique	16
4.2.2 Two-frequency technique	17
A. Background of the method	18
B. Measurements	19
C. Discussion of the obtained results	22
4.3 Measurement of a Bragg cell wavefront distortions	24
4.3.1 Measurements using a Hartmann-Shack wave-front sensor	25
A. Background of the method	25
B. Experimental setup	26
C. Estimation of the centroid error of spots	27
D. Experimental results and discussion	28
5. Conclusions	32
6. References	34

1. Introduction

Application of a Bragg acousto-optic cell in modern opto-electronic communication or measurement systems [1] often requires small phase distortions due to this cell. For instance, for broadband signals, nonlinearity of its phase response can result in considerable signal distortions, causing a noise increase or even a mistakenly transmitted word. In case of optical systems, a wave-front distortion caused by a Bragg cell, can significantly deteriorate their parameters. That is why the investigation of phase characteristics (phase response) of Bragg cells is practically important.

The present work is aimed to establish the relation of phase-response characteristics of Bragg cells with their constructive and technological parameters, as well as to study these characteristics experimentally.

One can imply different versions of a Bragg cell phase response depending on its application in a real system. To formalize the task, let us consider signal conversions in a heterodyne system with a Bragg cell.

Fig. 1.1 shows a general scheme of a Bragg cell use in a coherent opto-electronic system. An incident light wave $\mathbf{E}_i(\mathbf{r}, t)$ is converted by a Bragg cell into a diffracted (signal) wave $\mathbf{E}_B(\mathbf{r}, t, \omega)$. The latter is added to the reference light wave $\mathbf{E}_r(\mathbf{r}, t)$ on a beamcombiner. As usual, here \mathbf{r} is a radius-vector, t is time, $\omega = 2\pi f$, f is a frequency of an input radio-signal.

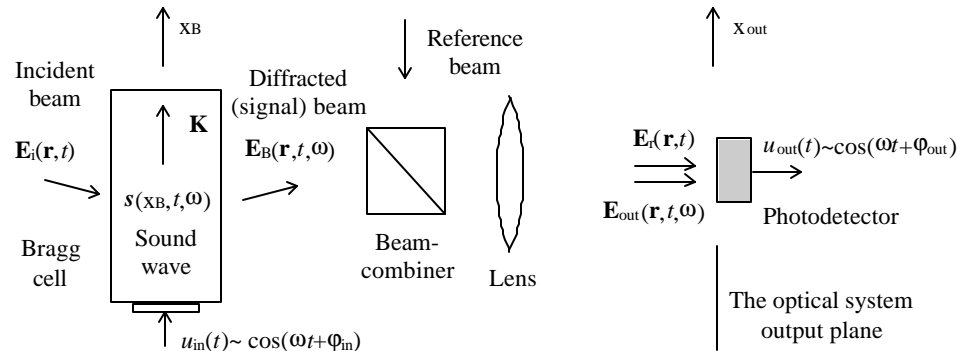


Fig.1.1. Signal conversions in a coherent heterodyne system with a Bragg cell.
 $\mathbf{E}_i(\mathbf{r}, t)$, $\mathbf{E}_B(\mathbf{r}, t, \omega)$, $\mathbf{E}_r(\mathbf{r}, t)$ - incident, diffracted and reference light waves correspondingly; \mathbf{K} - sound wave vector. $u_{in}(t)$, $u_{out}(t)$ - input (or driving) and output signals.

Having passed through the optical system of a photoreceiver (a lens in Fig. 1.1), both waves interfere on a photo-sensitive surface of a photodetector. At a harmonic input signal $u_{in}(t) \sim \cos(\omega t + \phi_{in})$, the frequency of a diffracted light wave differs from the frequencies of incident and reference light waves by a value ω . Therefore an output photodetector signal will be harmonic too: $u_{out}(t) \sim \cos(\omega t + \phi_{out})$.

It should be noted that there is no need to consider a concrete optical scheme in a general statement of problem. It is sufficient to suppose that a reference light beam is formed so to provide the wave-front matching condition [2, 3] for reference and signal light waves within overall frequency range. It is easily realized using a divergent reference beam [1, 4].

It is convenient to separate the problem of investigation of a Bragg cell phase-response onto two independent but connected parts. First, the whole opto-electronic device shown in Fig. 1.1 can be considered as a certain equivalent quadripole [4]. A non-dimensional transfer function of this quadripole

$$TF(i\omega) = U_{out}(\omega) / U_{in}(\omega) = TF(\omega) \exp(i\phi(\omega)), \quad (1.1)$$

where $U_{in}(\omega)$ and $U_{out}(\omega)$ are complex magnitudes of input and output signals at frequency ω , includes the phase response $\varphi(\omega)$ of the whole device which, as a rule, is an object of interest for a designer of integrated opto-electronic communication systems.

Secondly, the interest can be focused only on the wave-front distortions of an incident light wave $E(\mathbf{r}, t)$ inserted by a Bragg cell. Taking into account that these distortions can depend on frequency of a driving signal, it is reasonable to consider an "acousto-optic" transfer function

$$AOTF(i\omega) = E_B(\mathbf{r}, \omega) / E_i(\mathbf{r}) = AOTF(\omega) \exp(i\varphi_{AO}(\omega)), \quad (1.2)$$

where $E_i(\mathbf{r}, t)$ and $E_B(\mathbf{r}, t, \omega)$ are complex magnitudes of incident and diffracted light waves at a frequency of a driving electrical signal ω . In fact, the phase response $\varphi_{AO}(\omega)$ displays the wave-front distortions of an incident light beam depending on a sound frequency. This characteristic is important for designers of optical systems where a Bragg cell is used as a deflector, especially in phase-sensitive systems, rather than a device for data entry in an optical channel. Evidently, the distortions of a phase-response characteristic $\varphi_{AO}(\omega)$ must depend on the sound wave $s(x_B, t, \omega)$ characteristics and be incorporated in the distortions of a overall characteristic of $\varphi(\omega)$ as an additive component. Focusing on the Bragg cell application for coherent communication systems, we will concentrate on the studies of $\varphi(\omega)$ characteristic analyzing other "particular" characteristics (e.g., $\varphi_{AO}(\omega)$) only to get a deeper insight into mechanisms of physical processes in the system and to clarify reasons of arising phase distortions.

Thus, we have defined a phase response $\varphi(\omega)$ which is a subject of interest in the present work and, in fact, formulated an approach to measure this characteristic. Undoubtedly, this definition enables to develop a measurement procedure and then to obtain corresponding experimental results which allow to compare various Bragg cells. How these results should be used in practice depends on concrete application.

2. Calculation of a photodetector output phase (basic results of the first stage report)

To find an acceptable level of wave-front distortions of a signal light wave in a heterodyne optical system with a Bragg cell, the phase of the photodiode output depending on those distortions analyzed at the first stage of the work. Optical incident and reference beams with a Gaussian profile had been considered. An output signal phase had been investigated for different parameters of a Bragg cell in a regime of low acousto-optic efficiency. It was established that sound decay and truncation of an incident light beam did not practically affect the output photocurrent phase. But in some cases, irregular wave-front perturbations in the photodetector plane can result in considerable phase distortions of an output signal.

Briefly let us consider a way these results were obtained. The complex magnitude of an output signal regular component at some frequency f in one-dimensional case (i.e., after replacing $\mathbf{r} \rightarrow x_{out}$) is [2]

$$U_{out} = \int_{-a}^a E_{out}(x_{out}) E_r^*(x_{out}) dx_{out}, \quad (2.1)$$

where $E_{\text{out}}(x_{\text{out}})$ and $E_r(x_{\text{out}})$ are complex magnitudes of signal and reference light waves in the output plane of an optical system (see Fig.2.1), $2a$ is a size of a photodetector.

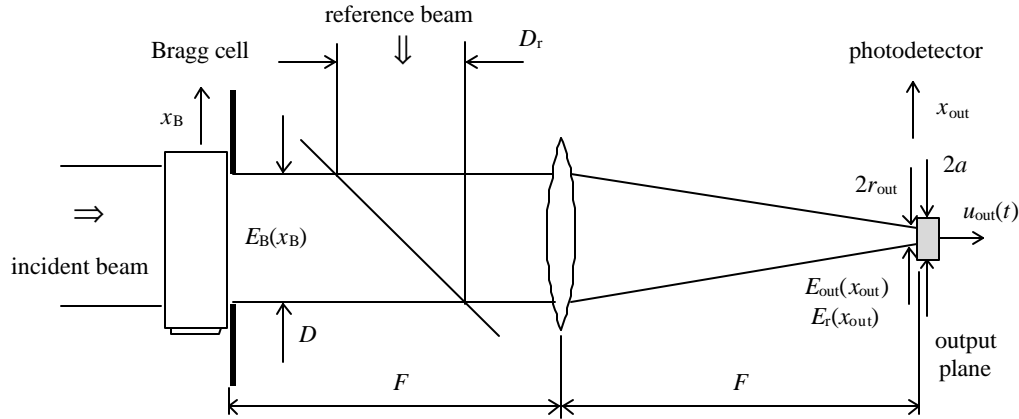


Fig. 2.1. The receiving part of a laser heterodyne system with a Bragg cell

Not accounting for some unessential constant term, one can write the expression for complex magnitudes [5,6]:

$$E_{\text{out}}(\bar{x}_{\text{out}}) = \exp[(\bar{\alpha}^2 / 4 - \bar{\alpha}\bar{x}_0) / 2] \cdot \exp(-\bar{x}_{\text{out}}^2 / 2) \cdot \exp[-i\bar{x}_{\text{out}}(\bar{x}_0 - \bar{\alpha} / 2 - \bar{D} / 2)] \\ \times \sqrt{\frac{\pi}{2}} \left\{ \text{erf} \left[\left(\bar{D} - \bar{x}_0 + \frac{\bar{\alpha}}{2} + i\bar{x}_{\text{out}} \right) / \sqrt{2} \right] - \text{erf} \left[\left(-\bar{x}_0 + \frac{\bar{\alpha}}{2} + i\bar{x}_{\text{out}} \right) / \sqrt{2} \right] \right\}, \quad (2.2)$$

$$E_r(\bar{x}_{\text{out}}) = \exp(-\bar{x}_{\text{out}}^2 / 2) \sqrt{\frac{\pi}{2}} \left\{ \text{erf} \left[\left(\bar{D}_r - \bar{x}_{0r} + i\bar{x}_{\text{out}} \right) / \sqrt{2} \right] - \text{erf} \left[\left(-\bar{x}_{0r} + i\bar{x}_{\text{out}} \right) / \sqrt{2} \right] \right\}, \quad (2.3)$$

where the lines above variables x_{out} , α , x_0 , and D denote that they are normalized on corresponding intensity ($1/e$) radii r_{out} or r_B of Gaussian beams in the output and Bragg cell planes. Here α is a frequency-dependent exponential-decay constant of acoustic intensity, D is an aperture of a Bragg cell, D_r is an objective aperture of the reference optical channel. The offset x_0 is included to allow the optical beam to be optimally placed within the Bragg cell aperture to increase the efficiency. The offset x_{0r} here, in fact, is always equal to $D_r/2$. Error function

$$\text{erf}(x) = 2\pi^{-1/2} \int_0^x \exp(-t^2) dt.$$

3. Designing of a Bragg cell with small phase distortions

3.1 Common considerations

To design a Bragg cell with small phase distortions to be used in an acousto-optic signal processing system, it is necessary to study how its parameters are connected with an output signal phase.

Usually a Bragg cell design procedure supposes that its construction parameters are to be chosen to achieve required technical characteristics. These parameters are the aperture of a Bragg cell D , the transducer length L and height H , and also the single crystal parameters: index of refraction n , sound velocity v , sound decay constant α , and figure of merit M_2 . An operating frequency f_0 , bandwidth Δf , efficiency η and resolution N have to be found as a result.

In Section 2, it was shown that a Bragg cell aperture and sound decay do not affect an output phase if there are no irregular perturbations of the diffracted light wave-front. Such perturbations can be caused

by various factors: non-homogeneity of optical properties of used material or technological inaccuracy of a Bragg cell fabrication. As a rule, these factors can be excluded if a technology is properly developed. But there is a physical reason which can not be excluded from consideration for any technologies used. This is temperature non-homogeneity which arises in a Bragg cell because of sound wave decay [8]. Obviously, it will be minimal if an acoustic power P_a is minimal, i.e. it is desirable to have an acoustic power as less as possible. On the other hand, at the same acoustic power the greater acoustic loss is, the greater an absorbed part P_{abs} of acoustic power is, i.e., a Bragg cell material should be chosen with a minimum sound decay constant α and a maximum figure of merit M_2 .

Often these requirements are contradictory: materials with a large figure of merit M_2 have also a large sound decay constant α . Therefore it is convenient to compare different materials considering the ratio of absorbed power to efficiency P_{abs}/η : the less this ratio is, the more a considered material is suitable. Taking into account that $P_{abs}=P_a(1-e^{-\alpha D})$ and $\eta=\sin^2[\pi/\lambda(P_aLM_2/2H)^{1/2}]$ [8], in case of low efficiency one can write

$$\frac{P_{abs}}{\eta} = \left(\frac{\lambda}{\pi}\right)^2 \frac{1 - \exp(-\alpha D)}{M_2} \cdot \frac{2H}{L}, \quad (3.1)$$

$\alpha D = \bar{\alpha}\bar{D}$, where normalized variables $\bar{\alpha}$ and \bar{D} have been defined in Section 2. When a Bragg cell is to be of high efficiency, the $\bar{\alpha}\bar{D}$ value has to be rather small. In fact, as it will be shown below, it has to be certainly less than 0.1. Under this condition one can write $\exp(-\alpha D) \approx 1 - \alpha D$, and in a first approximation the expression (3.1) becomes

$$\frac{P_{abs}}{\eta} \sim \frac{\alpha}{M_2} \cdot \frac{2H}{L} \cdot D. \quad (3.2)$$

That is, the simple ratio α/M_2 is a criterion to compare different materials: a better material has a less value of α/M_2 . One can also see that the expression (3.2) is useful to estimate an influence of constructive parameters: as usual, the ratio L/H should be maximum, but it is desirable the aperture D to be smaller to reduce the absorbed power. Evidently, it is desirable also to decrease an operating frequency f_0 to reduce acoustic loss.

What has been said is related to any Bragg cell. In some cases there exist additional factors causing phase distortions. For example, in a Bragg cell on TeO_2 the index of refraction for diffracted light wave depends on the angle, i.e. some frequency dependent error arises which is connected with a bandwidth Δf and should be taken into account. This error will be considered below.

3.2 Designing of a Bragg cell for a given efficiency

As it was shown in Section 2, in a heterodyne system, phase distortions caused by a Bragg cell weakly depend on acoustic loss and a Gaussian light beam truncation even if there are additional irregular phase perturbations of the diffracted light beam. Therefore its diffraction efficiency should be considered as a basic criterion for a design procedure. The efficiency value reduced because of truncation and acoustic loss can be calculated directly [6]:

$$\eta_{TL} = \eta_{AO} \exp(\bar{\alpha}^2 / 4 - \bar{\alpha}\bar{x}_0) \frac{\text{erf}\left(\bar{D} + \frac{\bar{\alpha}}{2} - \bar{x}_0\right) - \text{erf}\left(\frac{\bar{\alpha}}{2} - \bar{x}_0\right)}{2}. \quad (3.3)$$

At given values of $\bar{\alpha}$ and \bar{D} , the maximum diffraction efficiency η_{TLm} will be reached if \bar{x}_0 is equal to some optimal value \bar{x}_{opt} which can be found from the equation [6]

$$\begin{aligned} & \frac{1}{\sqrt{\pi}} \left[\exp(-(\bar{\alpha}/2 - \bar{x}_0)^2) - \exp(-(\bar{D} + \frac{\bar{\alpha}}{2} - \bar{x}_0)^2) \right] + \\ & + \frac{\bar{\alpha}}{2} \left[\operatorname{erf}\left(\bar{D} + \frac{\bar{\alpha}}{2} - \bar{x}_0\right) - \operatorname{erf}\left(-\bar{x}_0 + \frac{\bar{\alpha}}{2}\right) \right] = 0. \end{aligned} \quad (3.4)$$

Using (3.3) and (3.4), one can calculate a maximum reached efficiency of a Bragg cell as a dependence $\eta_{\text{TLm}}(\bar{D})$ considering the $\bar{\alpha}$ value as a parameter and assuming $\bar{x}_0 = \bar{x}_{0\text{opt}}$. Such dependencies are shown in Fig. 3.1. It is clearly seen from the figure that a desirable value of η_{TLm} can be reached only if $\bar{\alpha}$ is less and \bar{D} is more than certain values. Let us estimate what that means for a Bragg cell with acoustic loss equal to α [dB/ μsec] at some operating frequency. Taking into account that $\bar{\alpha}\bar{D} = \alpha D$ and $|10\lg(\exp(-\bar{\alpha}\bar{D}))| = 10\bar{\alpha}\bar{D} \lg e = 4.34\alpha D$, one can calculate a real aperture

$$D = 4.34 \cdot 10^{-6} \bar{\alpha} \bar{D} v / \alpha [\text{dB}/\mu\text{sec}]. \quad (3.5)$$

Then a maximum acceptable radius of a Gaussian light beam

$$r_B = D / \bar{D} = 4.34 \cdot 10^{-6} v \bar{\alpha} / \alpha [\text{dB}/\mu\text{sec}]. \quad (3.6)$$

A Bragg cell resolution

$$N = \Delta\theta / \delta\theta, \quad (3.7)$$

where the scanning angle $\Delta\theta = (\lambda / v \cos\theta_B) \Delta f$, θ_B is a Bragg angle. An angle divergency of a light beam $\delta\theta$ depends on the aperture D , on the light distribution across it, and on the criterion defining a light spot angle size. For an uniform distribution $\delta\theta = \lambda / D$ by the Rayleigh criterion and

$$N = \Delta f D / v \cos\theta_B. \quad (3.8)$$

In case of Gaussian distribution, light spots will be resolvable by Rayleigh [8] if $\delta\theta = \mu(w) \lambda / 2r_B$, where $\mu(w)$ is a parameter determined by a degree of a beam truncation which can be calculated at known ratio $w = D / 2r_B$. For example [8], $\mu = 1.16$ if $w = 1$, and $\mu = 0.86$ if $w \gg 1$. Thus, in this case using (3.6) and (3.7), one can write the resolution

$$N_{\text{GR}} = 8.68 \cdot \Delta f \cdot [\text{MHz}] \bar{\alpha} / \mu(w) \alpha [\text{dB}/\mu\text{sec}] \cos\theta_B. \quad (3.9)$$

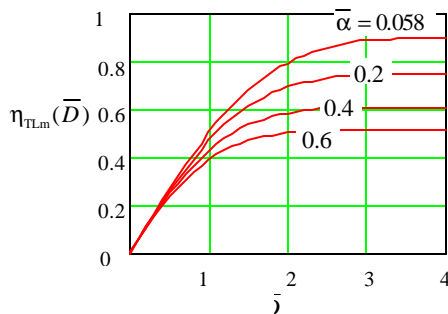


Fig. 3.1. Dependence of the overall efficiency of a Bragg cell on its normalized width at various sound decay factor $\bar{\alpha}$. The required value $\eta_{\text{TL}} = 0.9$ is reached only at $\bar{\alpha} \geq 0.058$, $\bar{D} \geq 3.7$; $\bar{x}_{0\text{opt}} = 1.519$ in this case.

Noting now the quantity $\bar{D}/2$ is exactly equal to the ratio w , one can say that a given value of the required efficiency η_{TLm} as well as a value of a sound decay constant α will determine a maximum resolution because it determines a value of \bar{D} . Let us estimate, for example, parameters of a Bragg cell with a given efficiency $\eta_{\text{TLm}} \geq 0.9$. This value of efficiency can be reached only if $\bar{\alpha} \leq 0.058$ and $\bar{D} \geq 3.7$ (see Fig. 3.1). Taking $\bar{\alpha} = 0.058$, $\bar{D} = 3.7$, $\cos\theta_B \approx 1$ and using (3.5), (3.6) we obtain a convenient expression to calculate a Bragg cell with efficiency $\eta_{\text{TLm}} = 0.9$:

$$D_{0,9}=9.31 \cdot 10^{-7} \nu / \alpha [\text{dB}/\mu\text{sec}]; \quad r_{B0,9}=2.52 \cdot 10^{-7} \nu / \alpha [\text{dB}/\mu\text{sec}]. \quad (3.10)$$

In this case the ratio $w=3.7/2=1.85$, that is the value of a parameter $\mu(w)$ should be within the range 0.86-1.16. Calculations give $\mu=0.89$ at $\bar{\alpha}=0.058$, $\bar{D}=3.7$, and $\bar{x}_0=1.519$. Then from (3.9) we obtain

$$N_{GR0,9} \approx 0.566 \cdot \Delta f [\text{MHz}] / \alpha [\text{dB}/\mu\text{sec}]. \quad (3.11)$$

3.3 Designing of a Bragg cell on TeO₂ with operating frequency $f_0=100$ MHz

Let us consider now a Bragg cell on TeO₂ with operating frequency $f_0=100$ MHz, bandwidth $\Delta f=30$ MHz and efficiency $\eta=0.9$ which has to be designed. A complete design procedure for such a Bragg cell is rather unwieldy and requires numerical simulation to be applied therefore we simply point out a reference [9] where it is described in detail. Using this procedure, the Bragg cell was designed to get following parameters:

light wavelength — $\lambda=0.633$ μm ; efficiency — $\eta=0.9$; frequency range — 85-115 MHz; other parameters had been taken to be arbitrary.

The designed (calculated) Bragg cell had the parameters as follows:

efficiency — $\eta=0.9$ at acoustic power 130 mw; frequency range — 81-116 MHz; output diffracted angles $\theta_{2\text{out}}$ (from the optic axis) — $-0.92^\circ \dots +0.94^\circ$; sound velocity — $v=686$ m/sec; construction angles (see Fig.3.2) — $\alpha_N=8.80^\circ$ and $\beta=4.12^\circ$; the transducer size — length $L=3$ mm and height $H=2$ mm.

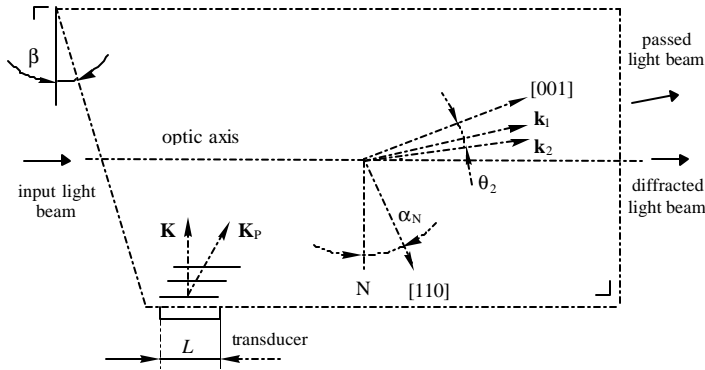


Fig. 3.2. Construction of a designed Bragg cell on TeO₂.

k_1 and k_2 - wave vectors of incident and diffracted light; K - wave vector of sound; K_p - Poynting's vector of sound; N - normal to the transducer.

Calculated frequency characteristic of the Bragg cell is presented in Fig. 4.6, Section 4 (curve 1).

Fig. 3.2. gives a sketch of its construction. The input face is tilted at the angle $\beta=4.12^\circ$ to provide a diffracted light beam parallel to the optic axis at some frequency (the calculated value was 98.3 MHz) in the middle of the frequency range.

The Bragg cell aperture and a Gaussian parameter of an incident light beam can be calculated from the condition $\eta=0.9$

using the relationships in the previous section. Having $\alpha=0.18$ db/ μsec at 100 MHz [6], and taking $\eta_{\text{TLm}}=0.9$ as a given value, from expressions (3.10)-(3.11) one can find for a designed Bragg cell: Aperture — $D=3.19$ mm, Gaussian light beam parameter — $r_B=0.86$ mm, resolution — $N_{\text{GR}} \approx 94$ at the bandwidth $\Delta f=30$ MHz.

Thus, it is necessary to increase Δf to get the resolution $N_{\text{GR}} > 100$. It results in an acoustic power growth because of L decrease and, hence, absorbed power will also increase in turn (see the expression (3.2)). That is, the simultaneous requirements to get a high efficiency and resolution, and to reduce wavefront perturbations are contradictory.

In the designed Bragg cell index of refraction for diffracted light beam depends on the angle of diffraction θ_2 (see Fig. 3.2), i.e. on its direction related to the optic axis [001]. Taking this fact into account, it was found using the design procedure mentioned above, that a phase difference of diffracted light wave at boundary values of frequency range did not exceed 16° at the light way length equal to 20 mm. As it was shown in Section 2, one can neglect such a value of a regular distortion.

3.4 Designing of a Bragg cell on GaAs

In many practical applications it is needed to have Bragg cells operating in the infrared range. A single crystal GaAs of $\bar{4}3m$ symmetry is suitable to design such Bragg cells because of its comparatively large value of M_2 and not very large sound decay α . This single crystal is optically isotropic, so that it has no frequency limitations except of those because of sound decay. In this case a design procedure is very uncertain if one does not mean any concrete application. For this reason we will only give an example to estimate in some way possible values of a Bragg cell parameters.

To chose a crystallographic orientation a phase distortions to be small let us estimate values of a parameter α/M_2 for different sound wave propagation directions.

For the longitudinal sound wave along the [110] direction the figure of merit $M_{2[110]}=104$ is known [10, 11] as well as sound decay $\alpha_{[110]}=22.5$ dB/cm at $f=1$ GHz [11]. Thus, $\alpha/M_{2[110]}=0.216$ for this direction.

For another suitable direction [111] the $M_{2[111]}$ value should be calculated. An effective photoelastic constant for this direction [12]

$$p_{\text{eff}}=(p_{11}+2p_{12}+4p_{44})/3. \quad (3.12)$$

Using data for photoelastic constants [13] $p_{11}=0.165$, $p_{12}=0.28$, $p_{44}=0.284$, we find $p_{\text{eff}}=0.243$. Taking values of sound velocity $v=5.1 \cdot 10^5$ cm/sec, index of refraction $n=3.4$, and density $\rho=5.3$ g/cm³ [13] we find $M_{2[111]}=135 \cdot 10^{-18}$ sec³/g. Having for this case the α value equal to 15 dB/cm at 1 GHz [13], we obtain the value of $\alpha/M_{2[111]}=0.111 < \alpha/M_{2[110]}=0.216$.

Thus, following the criterion formulated above (see the expression (3.2)), one can assert the direction [111] is more suitable to design a Bragg cell with small phase distortions. Below the calculation is made of a Bragg cell on GaAs for $\lambda=1.55$ μm at the same operating frequency $f_0=100$ MHz as the Bragg cell on TeO₂ designed earlier. The wavelength $\lambda=1.55$ μm is chosen because, firstly, many various semiconductor lasers for this wavelength are proposed by industry, and, secondly, the optical attenuation in GaAs at this wavelength is small enough [13].

Taking the efficiency $\eta=0.9$ should be obtained and having sound decay expressed in α [dB/ μsec] at 100 MHz is equal to 0.0765, one can directly use expressions (3.10), (3.11) to estimate parameters of a designed Bragg cell. Then its parameters calculated are:

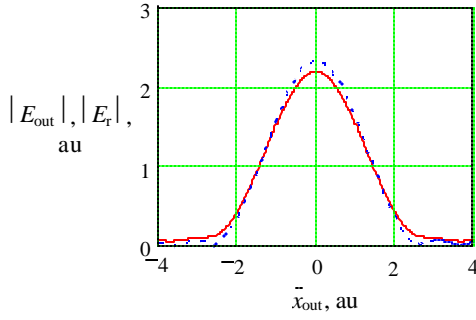
$D=6.2$ cm, $r_B=1.68$ cm and $N_{\text{GR}}=222$ at the bandwidth $\Delta f=30$ MHz.

In this case, the transducer optimal length determined for the -4 dB level of an amplitude frequency response, [8]

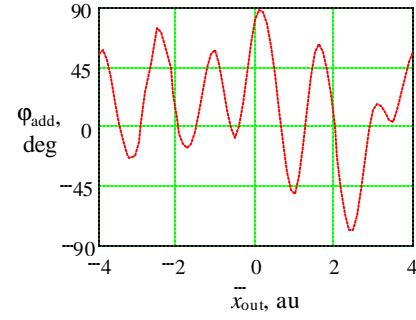
$$L \approx 1.56 \cdot v^2 n / \Delta f^2 \lambda. \quad (3.13)$$

Using values of v , n , Δf and λ pointed out above as given, we obtain the value of $L=9.9$ cm, i.e. the transducer length is obtained very large. Calculations show that even at non-uniformity of -1dB it will be greater than 3 cm. Thus, in a real device it can be chosen lesser to obtain a better uniformity of an amplitude frequency response. An ultimate conclusion how to chose constructive parameters and operating frequency of a Bragg cell on GaAs properly can be made only for a concrete application and after some preliminary experiments.

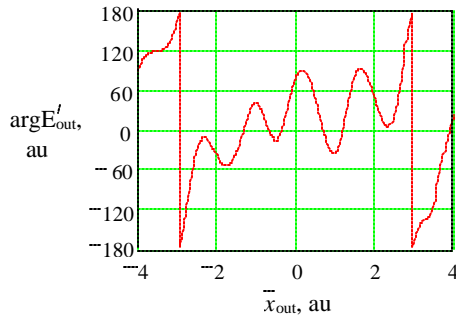
Some results obtained using (2.1)-(2.3) are presented in Fig. 2.2. The plots display what happens to an output signal phase when the wavefront of an output optical signal $E_{\text{out}}(x_{\text{out}})$ is perturbed by some "smooth irregular" function $\phi_{\text{add}}(x_{\text{out}})$. The function used in calculation is presented in Fig. 2.2, b. The limits of its variations are about



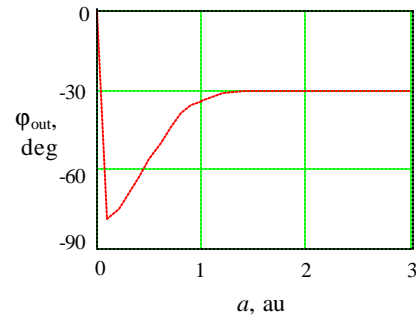
(a) - magnitudes of signal (red solid line) and reference (blue dot line) light beams



(b) - a perturbing function



(c) - the phase of a perturbed light beam



(d) the phase of an output signal

Fig. 2.2 The output phase ϕ_{out} vs a photodetector size a in case of some irregular wave-front perturbation of a signal light beam in the output plane.

$\pm 90^\circ$ that correspond to the wavefront distortions $\sim \lambda/4$, where λ is a light wavelength. It was added to the function $\arg(E_{\text{out}}(x_{\text{out}}))$ to form a perturbed function $E'_{\text{out}}(\bar{x}_{\text{out}}) = E_{\text{out}}(\bar{x}_{\text{out}}) \exp(i\phi_{\text{add}}(\bar{x}_{\text{out}}))$. The perturbed function obtained in this way is presented in Fig. 2.2, a (solid red line), and c (its magnitude and phase correspondingly). A complex magnitude $E_{\text{out}}(\bar{x}_{\text{out}})$ was calculated at $\bar{D} = 3.7$, $\bar{\alpha} = 0.058$ and $\bar{x}_0 = 1.519$. (Reasons to chose such parameters of a Bragg cell will be considered in Section 3). Complex magnitude $E_r(\bar{x}_{\text{out}})$ was calculated assuming $D_r = D$. Its phase was taken to be equal to zero and its magnitude is presented in Fig. 2.2, a (dot blue line). An output electric signal phase depending on the size of a photodetector $\phi_{\text{out}}(a) = \arg U_{\text{out}}(a)$ is presented in Fig 2.2, d. One can easily see that an output phase can have considerable distortions if a photodetector size is small (in the order of a light spot size in the output plane). That may be important when a phtodiode array is used, and reference probes are narrower than a signal mainlobe as it was considered in reference [1, p.119].

The performed analysis was related to the case when phase irregularities in the output plane had a smooth character. Apparently, this case seems to be rather rare. Practically it is more probable that such irregularities occur in

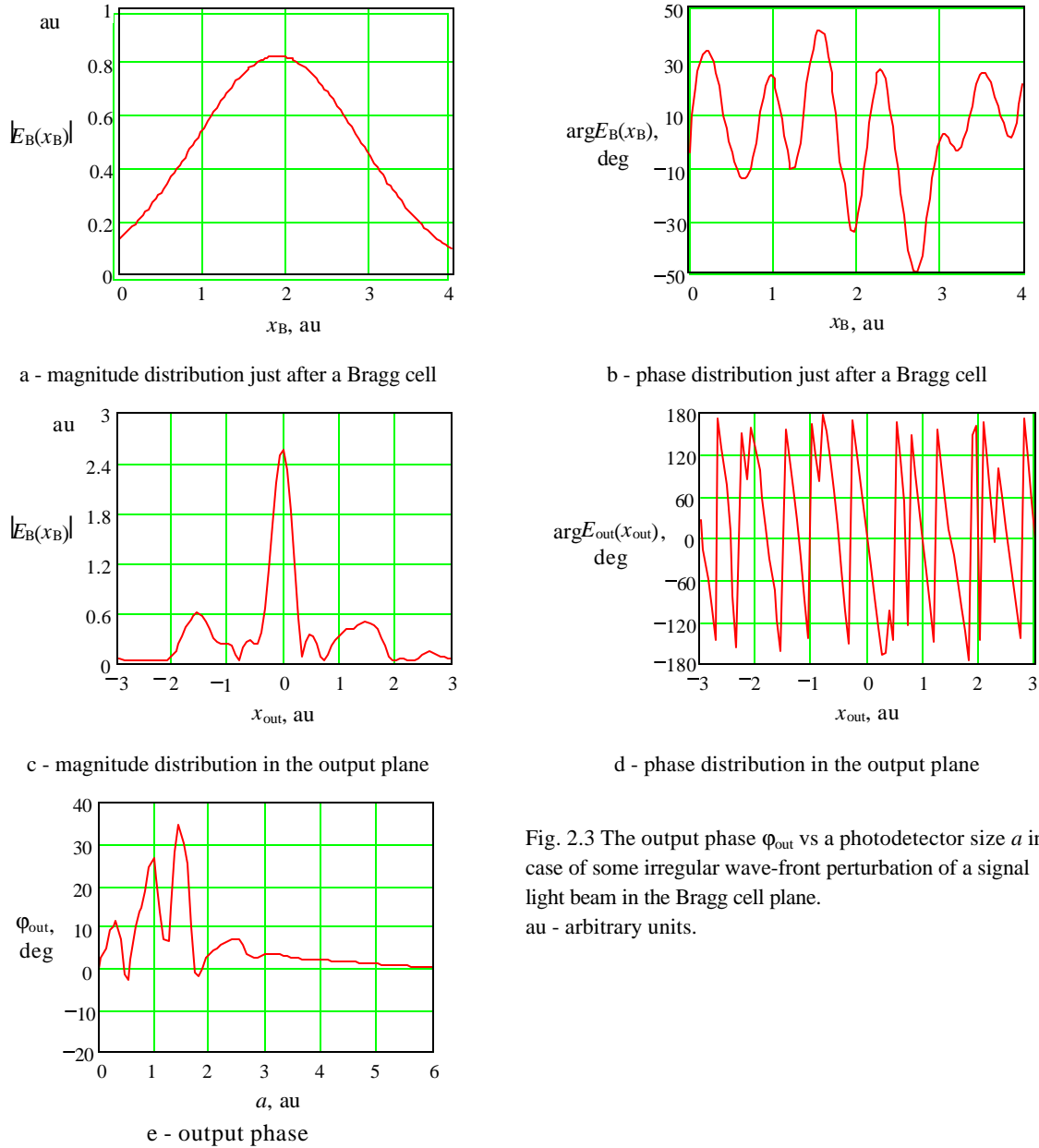


Fig. 2.3 The output phase ϕ_{out} vs a photodetector size a in case of some irregular wave-front perturbation of a signal light beam in the Bragg cell plane.
au - arbitrary units.

the Bragg cell plane rather than in the output plane because of, perhaps, non-homogeneity of optical properties of a used single crystal or technological inaccuracy of a Bragg cell fabrication. Such a case is considered below.

In Fig. 2.3, a, b the distribution $E_B(x_B)$ ¹ is presented in the diffracted light beam just after a Bragg cell. It is connected with the distribution $E_{out}(x_{out})$ in the output plane by the Fourier transform because the Bragg cell and output planes are located in the corresponding focal planes of a lens (see Fig. 2.1). In calculation, the magnitude distribution $|E_B(x_B)|$ (see Fig. 2.3, a) was obtained using the expression [6]

$$E_B(\bar{x}_B) = C \exp[(\bar{\alpha}^2 / 4 - \bar{\alpha} \bar{x}_0) / 2] \exp[-(\bar{x}_B - \bar{x}_0 + \bar{\alpha} / 2)^2 / 2] \text{rect}(\bar{x}_B / \bar{D}), \quad (2.4)$$

¹ Here arbitrary units (au) were used to count space coordinates. But they are the same in the pairs of plots: a-b and c,d-e. Thus, the size of a photodetector can be related to a size of a light beam spot in the output plane.

where C is a constant, and the asymmetric rectangle function ($\text{rect}(x)=1$ if $0 < x < 1$, $\text{rect}(x)=0$ otherwise) truncates the diffracted beam to within the width of the Bragg cell, which is assumed to have its transducer at the value $x_B=0$ and the end at the value $x_B=D$. It was calculated at the Bragg cell parameters $\bar{D} = 4$, $\bar{\alpha} = 0.202$ and $\bar{x}_0 = 2$.

Similarly to the previous case, the phase distribution had been constructed using some arbitrary "smooth irregular" function $\arg E_B(x_B)$ which was changed within the range $\pm 50^\circ$ (see Fig 2.3, b). A field in the output plane $E_{\text{out}}(x_{\text{out}})$ was calculated using Fast Fourier Transform (FFT), and its result is presented in Fig.2.3, c, d (magnitude and phase). A reference beam $E_r(x_{\text{out}})$ was taken to be real and equal to unit in the output plane.

The calculation result using (2.1) is presented in Fig.2.3, e. It is similar to that obtained in the previous case (see Fig.2.2, d), but a smooth character of a curve $\phi_{\text{out}}(a)$ has got broken. Apparently, one could expect that a complicated character of the $E_{\text{out}}(x_{\text{out}})$ distribution would result in considerable phase distortions of the output photocurrent. It should be noted, however, that an actual level of output phase distortions is unexpectedly low. Its maximum value is about 35° in spite of considerable phase variations on the photodetector surface (Fig 2.3, d). Of course, it is connected with an averaging effect of the photoelectric conversion which is described by the integral in (2.1). Also it is clearly seen that the output phase decreases to zero when the size of a photodetector becomes a few times more than a central light spot size.

In the way described above, the behavior of an output phase $\phi_{\text{out}}(a)$ was investigated at different parameters of a Bragg cell:

- 1) $\bar{\alpha} = 0$, $\bar{D} = 1.92$, $\bar{x}_0 = 0.96$, $\bar{D}_r = \bar{D}$, $\bar{x}_{0r} = \bar{D}_r / 2$;
- 2) $\bar{\alpha} = 0$, $\bar{D} = 3.0$, $\bar{x}_0 = 1.5$, $\bar{D}_r = \bar{D}$, $\bar{x}_{0r} = \bar{D}_r / 2$;
- 3) $\bar{\alpha} = 0.433$, $\bar{D} = 1.92$, $\bar{x}_0 = 0.96$, $\bar{D}_r = \bar{D}$, $\bar{x}_{0r} = \bar{D}_r / 2$;
- 4) $\bar{\alpha} = 0.361$, $\bar{D} = 1.92$, $\bar{x}_0 = 0.85$, $\bar{D}_r = \bar{D}$, $\bar{x}_{0r} = \bar{D}_r / 2$; sound decay through the Bragg cell width is equal to 3 dB.
- 5) $\bar{\alpha} = 1.199$, $\bar{D} = 1.92$, $\bar{x}_0 = 0.47$, $\bar{D}_r = \bar{D}$, $\bar{x}_{0r} = \bar{D}_r / 2$; sound decay through the Bragg cell width is equal to 10 dB.

As a result, it was established that a Bragg cell aperture and sound decay practically do not affect an output signal phase if a photodetector size is not considerably less than a central spot size.

Nevertheless, experimental investigations carried out in [5, 7], demonstrated qualitatively visible phase non-uniformities in the diffracted light beam. Thus, further quantitative measurements are necessary to conclude whether a Bragg cell application in opto-electronic or optical systems can result in considerable phase distortions.

4. Experiment

4.1 An experimental specimen

As an experimental specimen specially fabricated Bragg cell on TeO_2 was used, which was designed in Section 3. Its construction is presented in Fig. 3.2. The constructive angles α_N and β of the fabricated specimen were performed within the ± 5 angle second accuracy. The shear-wave transducer was fabricated from the LiNbO_3 plate which was bonded to a TeO_2 element by means of the vacuum diffusion welding, and then was grounded up to the required thickness. The surface opposite to the transducer was tilted at some angle to the sound wave-front and grounded to provide the reflected sound wave scattering and exclude its interaction with an incident light beam. No

back sound absorbers were used. The optical surfaces had flatness less than $\lambda/8$ which was tested using probing glass plate with flatness $\lambda/9$, and were antireflection coated for the Helium-Neon laser radiation. The reflection coefficient measured was less than 1%.

The Bragg cell was fabricated with the constructive angle α_N equal to 8.8° , which was chosen from the design procedure to obtain the required efficiency and frequency response in the range of 85-115 MHz. Its transducer had a surface $S=3(L) \sim 2 \text{ mm}^2$ and its operating frequency f_{tr} was equal to 97 MHz. It had been matched using the low pass

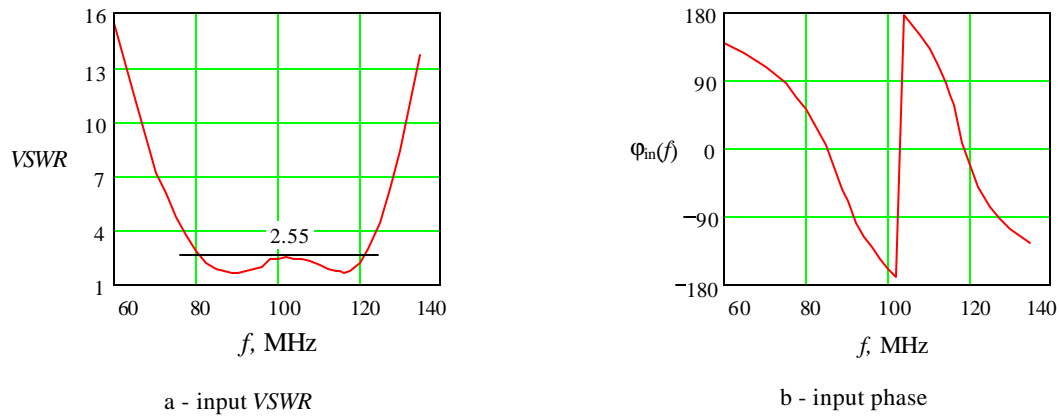


Fig. 4.1 VSWR and phase $\varphi_{in}(f)$ of the Bragg cell input reflectivity depending on frequency in the 50 Ohm radio channel.

filter section as a matching network. Its elements L and C were chosen to obtain the best characteristic of voltage standing wave ratio $VSWR(f)$ in the frequency range 85 - 115 MHz. The measured characteristic in the 50 Ohm radio channel is presented in Fig. 4.1. It has a bandwidth equal to 40 MHz (81 - 121 MHz) at the $VSWR$ level of 2.55. A measured phase $\varphi_{in}(f)$ of the input reflectivity of the matching network depending on frequency is presented in Fig. 4.1, b.

4.2 Measurement of a phase response $\varphi(f)$ of the equivalent opto-electronic quadripole

In this section, the techniques is considered to measure a phase response $\varphi(f)$ of the equivalent opto-electronic quadripole as it was defined in Section 1. Used definition has its advantages and disadvantages which will be discussed in Section 4.2.3, but in the present work just such measurements have been carried out.

4.2.1 Conventional technique

On the first stage, the experiments were carried out with a conventional (ordinary) technique. A phase response $\varphi(f)$ (see its definition in the expression (1.1)) had been measured directly comparing input and output electric signal phases by means of a RF phase meter. The experimental setup is presented in Fig. 4.2. It consists of an optical and an

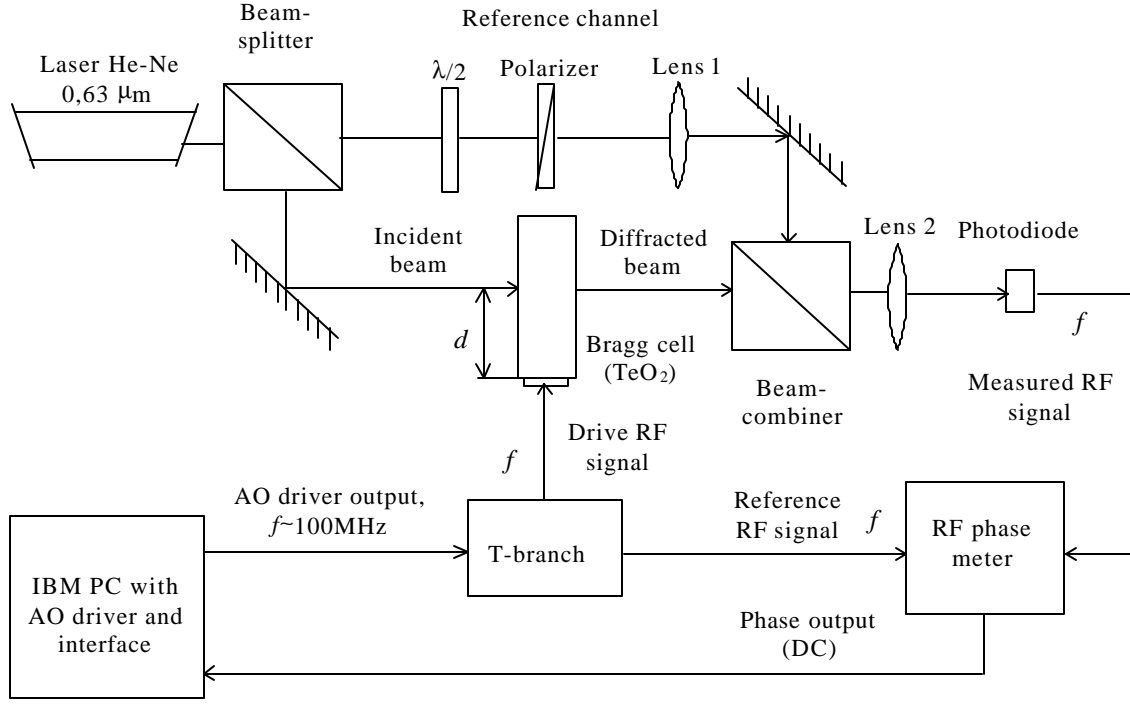


Fig. 4.2. Measurement setup using the Mach-Zehnder interferometer.

electric parts. The optical part has an architecture similar to the Mach-Zehnder interferometer. A Bragg cell on TeO_2 is mounted in one of its branches. Another branch is used to obtain a reference light beam for optical heterodyning. The light beam diffracted by the Bragg cell is added to the reference light beam using the beam-combiner. An output lens (lens 2) collects both beams on the photodiode surface. To provide the polarization of the reference beam the same as a polarization of a diffracted beam, a $\lambda/2$ plate together with a polarizer is used. A lens in the reference channel (lens 1) provides a wave-front matching condition in a wide frequency range. A harmonic electric signal of frequency f from the AO driver comes to the T-branch where it branches into the drive signal for a Bragg cell and the reference one for the RF phase meter. Since a diffracted light frequency is shifted by frequency f relatively to frequency of the reference beam, the photodiode output phase of frequency f can be compared with a phase of the reference RF signal. Thus, when a frequency is changed within some frequency range, the phase meter output gives directly a phase response of the equivalent opto-electronic quadripole $\varphi(f)$, which was defined by the expression (1.1).

In such a way pictures were recorded which displayed the dependencies $\varphi(f)$ within very narrow frequency ranges about frequencies 75 and 95 MHz (see Fig. 4.3). In the pictures, brightness from white to black shows a phase changing within a range of $\pm 180^\circ$ which are the limits of the phase meter measured values. The x -coordinate displays nothing: it is only connected with a way used to record a phase variations. Unfortunately, they display only some qualitative features of a Bragg cell. As we will see below, there is no possibility to measure its quantitative characteristics in this way.

Really, considering the pictures, one can see that there is a number of phase skips of the $\pm 180^\circ$ value (from black

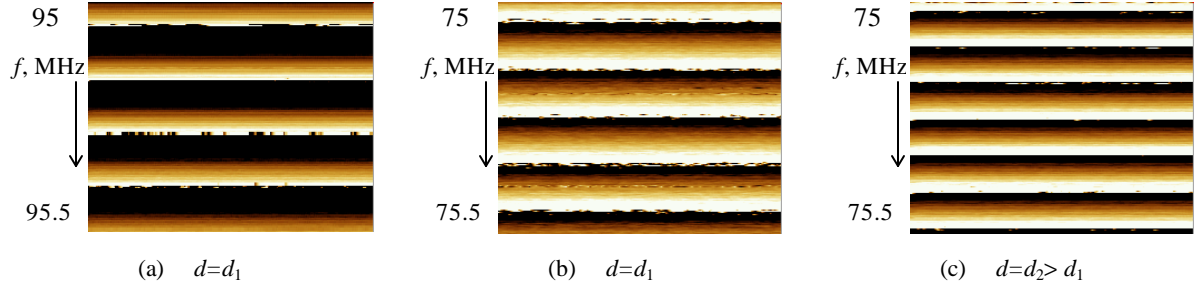


Fig. 4.3. Displayed dependencies of an output phase on frequency. One can see a different number of phase skips at the same frequency changes and different distances. d - a distance between a transducer and an incident light beam.

to white) within a frequency range of 0.5 MHz. That is, a slope of a phase response is so steep that a slight frequency change results in a significant change of an output phase. One can show that it happens mainly because of a sound wave delay in a Bragg cell. Indeed, in Fig. 4.3 (b) and (c) pictures were recorded within the same frequency range. The difference is only that the picture (c) was recorded when an incident light beam passed the Bragg cell at a distance d from the transducer (see Fig 4.3) which was greater than in the picture (b). It is well seen that the greater a distance d is, the steeper the slope of a phase response $\phi(f)$ is (a greater number of observed phase skips is). That is, we will obtain different results recording those characteristics at slightly different frequencies f (and, of course, at different d). Thus, the described effect will result in uncertainty in measured phase values at different frequencies unless the special procedure is applied to count a number of phase skips during a continuous frequency variation. In the case of arbitrary frequency samples as it is usually during digitizing, such a procedure is simply impossible.

In fact, the conventional technique allows to make necessary measurements only in a very narrow frequency range. Thus, one has to change the way and the approach to measure a phase response $\phi(f)$. A new approach which allows to measure it in the wide frequency range is described below.

At the same time, the experiment carried out gave some useful information. Fig. 4.3 (a) presents a picture recorded at the same distance d as in (b). One can see that slopes of a phase response are different in these cases (different number of skips), that is its slope depends on frequency in a wide frequency range.

4.2.2 Two-frequency technique

As it was shown above, it is impossible to measure a phase response $\phi(f)$ in a wide frequency range with the direct conventional technique using a RF phase meter. But there is a possibility to avoid the "effect of phase skips" measuring a group delay time instead of a phase. Therefore a new two-frequency method for measuring a Bragg cell phase response $\phi(f)$ was developed which is based on this well known principle. Its basic advantages are:

- 1) to make measurements using an arbitrary frequency samples, i.e. to apply a standard digital techniques;
- 2) frequency translation of measured signals into a low frequency range allow to simplify a measurement equipment and to increase a measurement accuracy.
- 3) one does not need to use a special high frequency photodiode (100 MHz).

A. Background of the method

It is well known that a group delay time τ in some linear system is connected with its phase response by the following relation:

$$\tau(\omega_0) = |d\varphi(\omega)/d\omega|_{\omega_0}, \quad (4.1)$$

i.e., one can measure a group delay time $\tau(f)$ depending on frequency f within some frequency range $f_{\text{low}}, f_{\text{high}}$. In fact, it is possible to measure directly a phase derivative $d\varphi(f)/df \approx \delta\varphi(f)/\delta f$ measuring a difference $\delta\varphi(f) = \varphi(f_1) - \varphi(f_2)$ at some frequency difference $\delta f = f_1 - f_2$, and then calculate a phase response $\varphi(f)$ from the expression

$$\varphi(f) = \int_{f_{\text{low}}}^f \frac{\delta\varphi}{\delta f'} df', \quad (4.2)$$

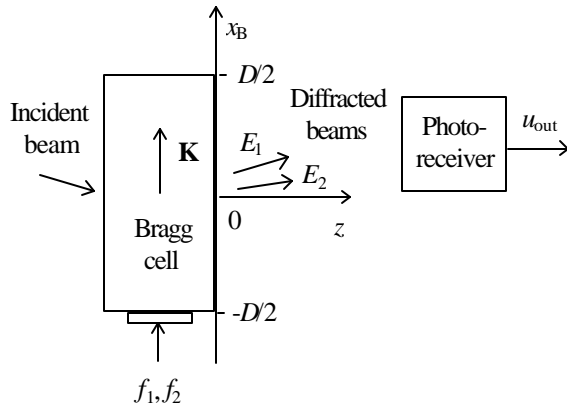


Fig. 4.4 The model to calculate an output signal phase of a difference frequency δf .

where f' is the dummy variable of integration. It is evident that the characteristic $\varphi(f)$ will be calculated up to a constant, because the integral in (4.2) will be equal to zero at frequency $f = f_{\text{low}}$. Necessary conditions to properly measure a characteristic $\varphi(f)$ in this way are $\delta_0\varphi \ll \delta\varphi$ and $\delta f \ll f$, $\delta_0 f \ll \delta f$, where $\delta_0\varphi$ and $\delta_0 f$ are a measurement error of $\delta\varphi$ and an error of a frequency set, correspondingly.

The simplest way to measure $\delta\varphi(f)/\delta f$ is to apply simultaneously two signals with close frequencies directly to a Bragg cell, then to mix two diffracted light beams on the surface of a photodetector, to extract the signal of a

difference frequency δf from its output, and finally, to measure its phase. But to be sure that a measured value is exactly the same as in the case of ordinary (conventional) heterodyne architecture, we need to substantiate a proposed approach.

Consider the simplest model describing signal conversions in a heterodyne system with a Bragg cell when there are its two input signals with close frequencies f_1 and f_2 (Fig. 4.4). Incident light beam is diffracted by two sound waves of those frequencies into two light beams E_1 and E_2 . These beams propagate at slightly different angles to the z axis and then are collected by a photoreceiver (e.g., by a photodiode together with some optical system) deriving an output electric signal of frequency δf . Apparently, some additional phase difference $\delta\varphi_0$ should arise from that angle difference. Let us calculate it.

Magnitudes of diffracted light waves E_1 and E_2 can be written in form [3,4]

$$E_{1,2} = \exp(-i[(\omega_{\text{light}} + \omega_{1,2})t - K_{1,2}(x_B + D/2) + \varphi_{S1,2}]), \quad (4.3)$$

where ω_{light} is a cycle light frequency, $\omega_{1,2} = 2\pi f_{1,2}$, $K_{1,2}$ - sound wave numbers, $\varphi_{S1,2}$ - initial phases of sound waves. Then, having taken the all light to be collected by a photoreceiver, one finds a complex analytical output signal

$$\begin{aligned}
u_{\text{out}} &= \int_{-D/2}^{D/2} E_1(x_B) E_2^*(x_B) dx_B = \\
&= \exp[i(\omega_1 - \omega_2)] \exp[i(\phi_{s1} - \phi_{s2})] \exp[i(f_1 - f_2)\pi D / v] \frac{\sin[(f_1 - f_2)\pi D / v]}{(f_1 - f_2)\pi D / v},
\end{aligned} \tag{4.4}$$

where E_1 and E_2 are complex magnitudes of diffracted light waves, v is a sound velocity. The first exponential term here simply displays a fact that an output signal is harmonic of frequency δf . The second one shows a difference between two sound wave phases. But the third term is exactly that which is connected with a way we obtain an output signal, i.e. the phase addition $\delta\phi_0$ arising because of the angle difference of the diffracted light wave directions:

$$\delta\phi_0 = (f_1 - f_2)\pi D / v, \tag{4.5}$$

This is a constant error of the method. As it is seen from the expression (4.5), it is directly proportional to a frequency difference δf and a delay time $\tau_b = D/v$ of sound wave in a Bragg cell. Therefore one needs to chose δf smaller to reduce the constant error, or it must be taken into account in calculations of measured values.

The last term in the expression (4.4) (of form $\sin x/x$) represents the condition similar to one known in the optical heterodyning theory [2] as a condition of wave-front matching: the less a frequency difference is (i.e., the less an angle between two diffracted light beams is), the more an output signal is.

Thus, from all the reasons, it is necessary to take a frequency difference δf as small as possible.

B. Measurements

To practically realize the developed method, a special experimental setup was constructed which is presented in Fig. 4.5. Its optical part included a tested Bragg cell, He-Ne laser (0.633 μm), two lenses, and a photodiode together with a prime-amplifier as basic elements. Laser output power was 1 mw, the light beam diameter on the output mirror was equal to 0.8 mm. There were also used some additional elements: attenuators, space filters and a telescope as they were needed. One of the back and front focal planes of two lenses were joined. A Bragg cell and a photodiode were located in the other planes. Such a configuration transferred a Bragg cell scanning center onto the surface of a photodetector. That is, a photodetector did not need to be moved while a drive frequency f changed. Thus, a possibility was realized to measure a Bragg cell phase response within a wide frequency range not having changed positions of all optical elements.

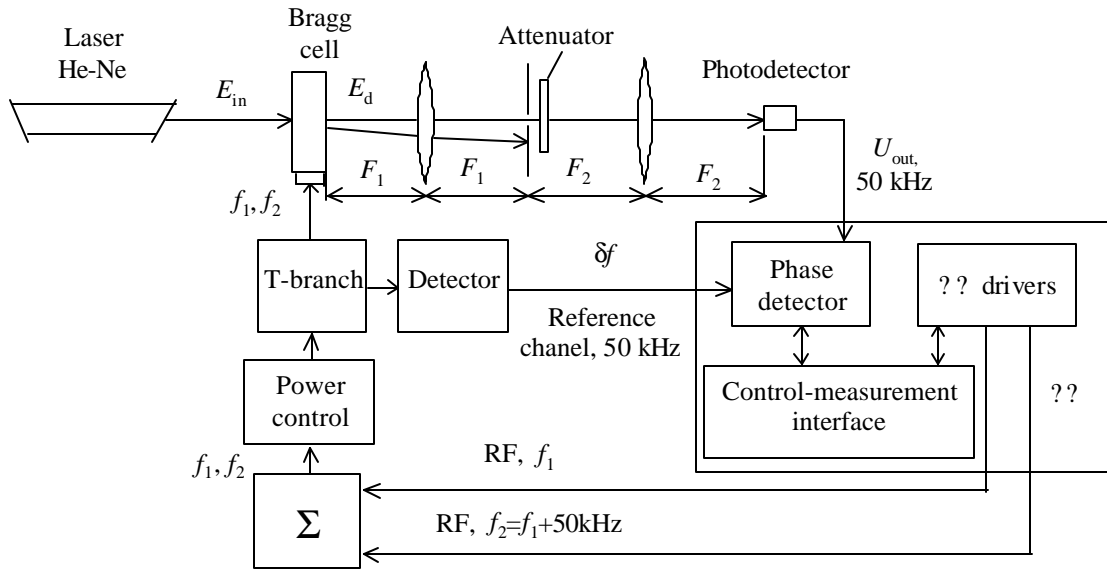


Fig. 4.5. The measurement setup using two frequency technique.

The electric part was designed so to take the low frequency (50 kHz) reference signal equal to δf directly from the input of a Bragg cell. Under this condition, a measured phase response had to be exactly as one defined by the expression (1.1). Two synthesizers of direct synthesis were used in the two drivers of a Bragg cell (AO drivers), so that their output frequencies had an accuracy and stability of quartz. One of the output frequencies (the basic one) was equal to a given frequency f , and another one was shifted from that by the frequency $\delta f = 50$ kHz.

Two output signals of AO drivers came onto an adder, and then a summed signal, passing an output power controls, was branched into a Bragg cell directly and into a detector. Thus, the detector was located directly at the Bragg cell input. The detector output of difference frequency δf was used as a reference signal for a specially designed digital phase detector.

An output signal of frequency δf from a photodetector was the measured signal. Within an arbitrary frequency range which could be chosen anywhere from 65 to 130 MHz, 512-frequency samples were given by a special program on IBM PC. The program also simultaneously controlled AO drivers and the measurement system. A 2D array, of given frequencies f and measured values of $\delta \phi$, was obtained as a result.

The experimental setup was calibrated and tested. It was established that within a frequency range of 75-125 MHz, a phase difference $\delta \phi$ was measured with accuracy of $\pm 3^\circ$.

The same experimental setup was used to measure a Bragg cell efficiency $\eta(f) = I_1/I_{in}$ depending on frequency. Here I_{in} is an incident beam efficiency, I_1 is an efficiency of the first diffraction order. The shifted frequency channel was made to be turned off when the frequency response (FR) $\eta(f)$ of the fabricated Bragg cell was measured. It is presented in Fig. 4.6 (curve 2). It was measured at the input electric power of 130 mw to achieve a maximum efficiency equal to 0.89. Curve 1, Fig. 4.6 shows the characteristic calculated in Section 3. The Bragg cell was designed for an efficiency of 0.9 and the bandwidth 81-116 MHz at this efficiency value. Calculated and measured results are shown to be in a good agreement. The real Bragg cell had the minimum efficiency equal to 0.86 within the bandwidth of 81.7-114.2 MHz, i.e. its FR had non-uniformity of 4%.

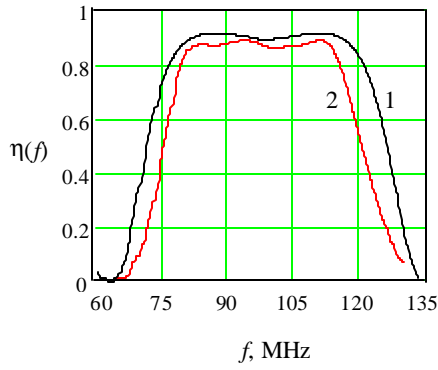


Fig. 4.6. Efficiency $\eta(f)$ vs frequency of the fabricated Bragg cell

For phase measurements, a Bragg cell position was fixed so that the $\eta(f)$ characteristic of Fig. 4.6 was maintained the same, and then dependencies $\delta\varphi(f)$ were measured. Dependencies $\varphi(f)$ were calculated using (4.2) and taking into account the constant error $\delta\varphi_0$ according to (4.5) (it was subtracted from measured $\delta\varphi(f)$ values). Results obtained at different parameters of acousto-optic interaction are presented below. In Fig. 4.7 characteristics at different input power levels P_{in} are presented which were obtained at the diameter of a laser beam of about 1 mm. They are practically identical except some differences within the frequency range 88-98 MHz and above 120 MHz. It was found out, the

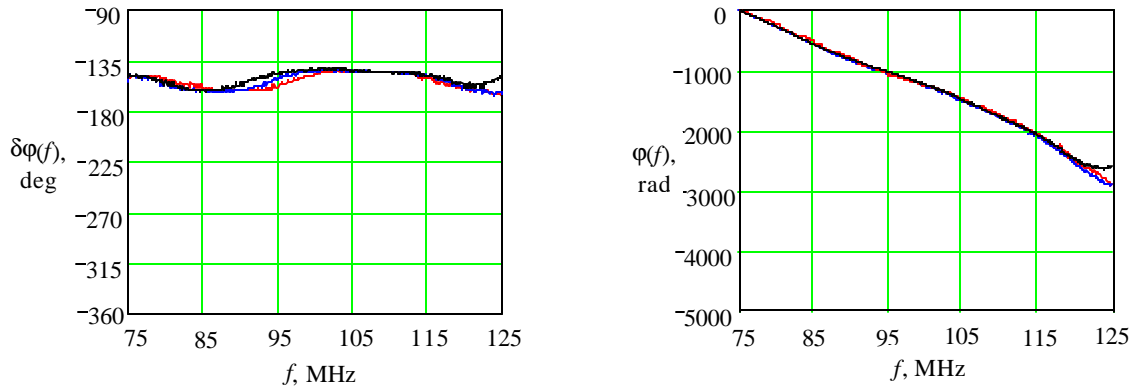


Fig. 4.7. Measured characteristics $\delta\varphi(f)$ and calculated using (4.2) phase responses of the Bragg cell $\varphi(f)$ at different input power levels P_{in} . Red - $P_{in}=100$ mw, blue - $P_{in}=50$ mw, black - $P_{in}=10$ mw.

first difference is connected with features of a used detector. The second difference arises because of a low intensity of diffracted light beam at small input power $P_{in}=10$ mw at frequencies above 120 MHz, practically beyond the Bragg cell bandwidth. Thus, one can definitely claim that measured phase responses do not depend on input power

From that reason all further measurements were carried out at the same input power equal to 50 mw.

Note also that the plot for characteristics $\varphi(f)$ is made in terms of radians for y-axis. It shows that the measured slope of a Bragg cell phase response is very steep, in the order of 9000 deg/MHz. Exactly the same was qualitatively perceived in Section 4.2.1. Obviously, such a steepness is mainly determined by a sound wave delay in the Bragg cell.

Fig. 4.8 shows the results obtained at different positions of an incident light beam related to the transducer, i.e. at different distances d (see Section 4.2.1). As earlier, dependencies $\delta\varphi(f)$ were measured, then characteristics of the delay time $\tau(f)$ and $\varphi(f)$ were calculated using (4.1) and (4.2). As in the previous case, the diameter of an incident light beam was equal to ≈ 1 mm for curves 1-3, and had the equivalent size of 4 mm for the curve 4. Curve 1 was obtained at some distance $d=2-4$ mm (it was not measured exactly). Curves 2 and 3 were obtained at exact distances $d_1=d+2$ mm and $d_2=d+3$ mm (with accuracy of ± 0.02 mm). The curve 4 was obtained when an input telescope was mounted just after the laser.

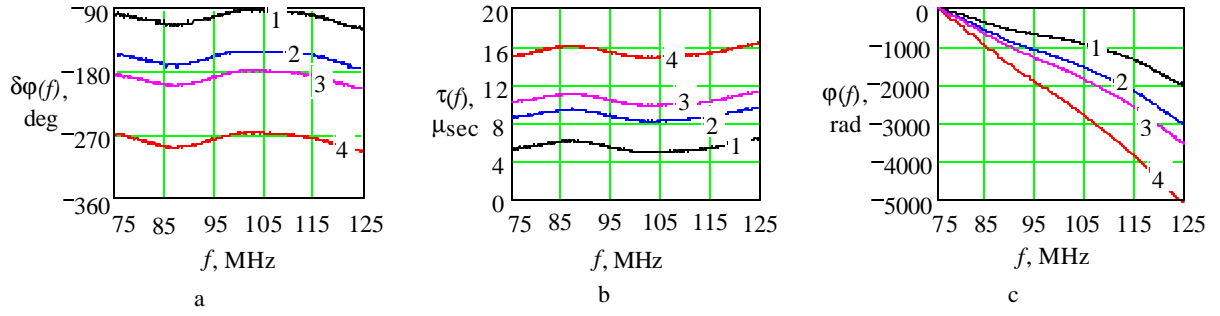


Fig. 4.8. Measured characteristics $\delta\phi(f)$ at different distances d of an incident light beam from the transducer. The delay time $\tau(f)$ and phase responses $\phi(f)$ were calculated using (4.1) and (4.2). The diameter of the beam is equal to ≈ 1 mm for curves 1-3, and ≈ 4 mm for the curve 4. The curve 1 was obtained at some distance d , the curves 2 and 3 at distances $d_1 = d+2$ mm and $d_2 = d+3$ mm. Input power $P_{in} = 50$ mw.

C. Discussion of the obtained results

One can see from Fig. 4.8 that obtained dependencies are identical except a different slope of phase responses. Obviously, mainly it occurs because of a different sound wave delay in the Bragg cell and its different apertures and does not matter in most applications. In practice however, that can result in some problems when two various Bragg cells are used in the same opto-electronic system. Really, if one of them is used in the reference channel instead of a lens (see Fig. 4.2) to create a number of reference beams as it is described in [1, p. 114], and has an aperture different from a Bragg cell aperture used in the signal channel, then a considerable phase dependence on frequency can arise in an output signal of a photodetector. Apparently, it will be linear, but in fact, result can be uncertain in some cases which were investigated in Section 2.

It is also important to note, that obtained results demonstrate an explicit dependence of a delay time τ on frequency (see Fig. 4.8, b). One can surely say, this fact is unexpected and requires a discussion. Really, there seems to be no reason why it should be. The experimental setup was carefully calibrated and tested. Theory [8, 11, 14, 15] also does not give any predictions. Therefore some additional measurements were necessary to clarify the situation. They were carried out and the results are presented below. Prior to consider them, let us return for a moment to the common approach formulated in Section 1.

As follows from the definition of a phase response $\phi(f)$ (see expression (1.1)), the measurements described above were carried out comparing complex input and output signals $U_{in}(f)$ and $U_{out}(f)$. That is, an input signal was directly used as a reference. In this case, a measured value $\delta\phi$ would have some phase additive error $\delta\phi_{err}(f)$ if there existed a frequency dependence of the input signal phase. Such a dependence has to undoubtedly exist because the input VSWR of the investigated Bragg cell is not exactly equal to unit over the frequency range and the input reflectivity phase $\phi_m(f)$ obviously depends on frequency (see Fig. 4.1). In other words, the input signal depends on the input impedance $Z_{in}(f)$ of a Bragg cell: $U_{in} = U_m(f, Z_{in})$. Apparently, to exclude the effect, a directional coupler could be applied instead of a T-branch in the measurement scheme of Fig. 4.5. Then the direct wave $U_{drc}(f)$ would be used as a reference whose phase does not depend on the input impedance $Z_{in}(f)$. In addition, if the observed frequency dependence $\delta\phi(f)$ were only determined by a reference phase dependence, then the effect should disappear (of course, if there were no distortions of phase response of a directional coupler). The modified part of the measurement scheme in this case is shown in Fig. 4.9, a. It is a desirable modification, but there was used a different one in the experiment (Fig. 4.9, b): instead of a directional coupler, an attenuator was used between a T-branch and a Bragg cell.

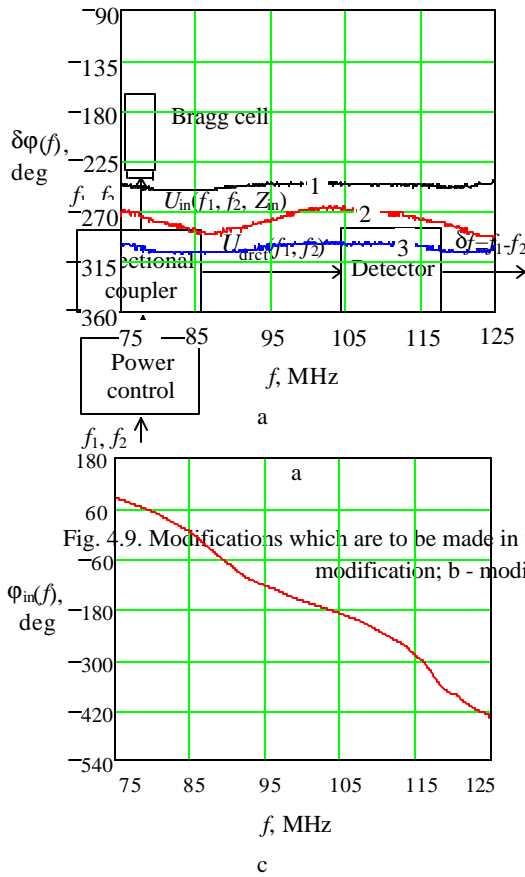


Fig. 4.9. Modifications which are to be made in the measurement setup presented in Fig. 4.5; a - desirable modification; b - modification used in the experiment; c - phase of the Bragg cell input reflectivity depending on frequency in the 50 Ohm radio channel.

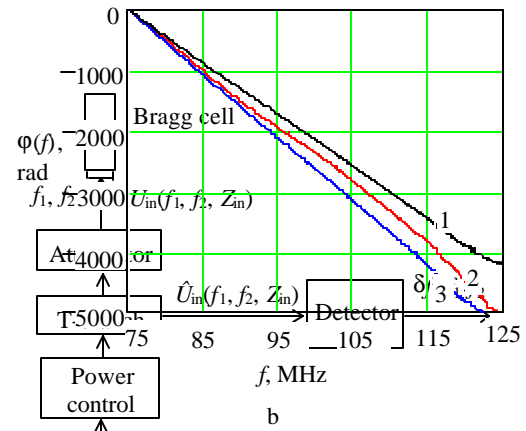


Fig. 4.10. a - measured characteristics $\delta\varphi(f)$ obtained using various attenuators: curve 1 - 10 dB, curve 2 - 6 dB; b - phase responses $\varphi(f)$ were calculated using (4.1) and (4.2). The diameter of an incident beam is equal to 4 mm. Input power in the experiment: curve 1 and 50 mw for curves 2 and 3; c - phase of the Bragg cell input reflectivity depending on frequency in the 50 Ohm radio channel.

Of course, in this case a reference $\hat{U}(f_1, f_2, Z_{in})$ also depends on a Bragg cell input impedance $Z_{in}(f)$, but this dependence is reduced because of the attenuator. A degree of the reduction is determined by an attenuation value.

As described, measurements were made repeatedly. The results are presented in Fig. 4.10. An incident beam diameter was approximately equal to 4 mm (see also Fig. 4.8, curve 4). Attenuators with the attenuation of 6 dB (curve 3) and 10 dB (curve 1) were used. Curve 2 describes a case when attenuation was equal to zero. There is clearly seen a smoothed frequency dependence of a measured $\delta\varphi(f)$ value: the greater an attenuation is (curve 1), the more smooth the curve is. It is evident that observed non-uniformities of measured dependencies $\delta\varphi(f)$ are really determined by a character of frequency dependence of the input impedance $Z_{in}(f)$. It is also confirmed from a comparison of curve 2 in Fig. 4.10,a, with a curve in Fig. 4.10,c which is the same characteristic $\varphi_{in}(f)$ as in Fig. 4.1,b, but presented in a form convenient for comparison. Visible correlation between them is well seen. It also should be noted, the aforesaid is related to frequency dependencies but not to absolute measured values of $\delta\varphi$. Observed difference in them (see Fig. 4.10, a) which has led to a difference in phase responses $\varphi(f)$ (see “a fan” in Fig. 4.10, b), apparently is connected with different phase features of used attenuators. At the same time, a linearity of curves 1 and 3 (with attenuators) is much better than of curve 2 (with no attenuators).

Thus, one can certainly claim that observed non-uniformities in measured dependencies $\delta\varphi(f)$ are connected with the used approach and definition of a phase response according to the expression (1.1). The measurement procedure has been constructed to obtain exactly a phase response $\varphi(f)$. A consequence of that is that obtained values of a delay time have become strongly depending on the input impedance of a Bragg cell, i.e. on frequency. Correspondingly, and a phase response $\varphi(f)$ itself has become nonlinear. To conclude, whether the applied definition is suitable or not, one can only considering a concrete case of a Bragg cell application in practice.

4.3 Measurement of a Bragg cell wave-front distortions

As it is clear from the results presented above, sound decay and truncation of an incident light beam in a Bragg cell did not practically affect the output photocurrent phase. But irregular wave front perturbations in the photodetector plane, if exist, can result in considerable phase distortions of an output signal. For this reason it is of great interest to investigate in a direct way the uniformity of a diffracted beam. In this section we present an analysis of wave front sensing, having a common use in adaptive optics, as applied to a Bragg cell phase distortions.

A first technique could be applied is to deduce the phase φ from the intensity distribution in the focal plane. The distribution for a point source is the point spread function which is the Fourier transform of the optical transfer function. This inverse problem is so-called phase problem in optics [16]. There is no unique solution in the general case, and measurements and/or a priori constraints must be used. The Gershberg-Saxton iterative algorithm is the basic principle of the technique [17]. The main drawbacks of these methods are the requirement of really point source which is difficult to provide in practice, and the computing time.

The most popular optical techniques to sense the wave front is based on the interferometric methods. There is a lot of methods based on interferometry. The principle is to form a fringe pattern between the beam coming from the test object and the beam coming from the reference mirror. The main disadvantage of the device in a Bragg cell testing is the requirement for the identity of reference and tested beam frequencies. Because of diffracted wave frequency shifting, observed fringe pattern is unstable, and its registration is difficult. In addition, the restoration of phase distribution is complicated by speckle in formed interferogram.

A very powerful approach to the problem is direct wave front testing by means of sensors widely used in adaptive optics. This technique is used now for testing mirrors and lenses, in remote sensing and ophthalmology. It permits not only direct wave front measurements, but real-time correction of its distortion, as well. As the wave-front measurement method we adopted the Hartmann-Shack sensor [18,19] which is optimal for testing large-aperture optical devices. The main advantages for wave front measuring with Hartmann-Shack sensor are as follows. First, in contrast to interferometric methods, one can produce a reference beam quite easy by simple telescopic system with spatial filtration in a focal plane. Second, because wave front distortion is in inverse proportion to the magnifying power, the larger the beam aperture becomes, the higher the measurement accuracy can be obtained. Third, because Hartmann-Shack sensor measures the local wave front slope, one can achieve a wave-front correction directly by wave front control, using individual actuators on a deformable mirror or liquid-crystal spatial light modulator.

In this section, we give the brief description of optical setup used in our investigation, and the analysis of main measurement errors of the device. The results received with the designed Bragg cell on TeO_2 and a short discussion concludes the section.

4.3.1 Measurements using a Hartmann-Shack wave-front sensor

A. Background of the method

The principle of the Hartmann-Shack wave-front sensor is well known [19]. A lenslet array is placed in a conjugate pupil plane in order to sample the incoming wave front. If the wave front is plane, each lenslet forms an image of the source at its focus. If the wave front is disturbed, a lenslet received an inclined wave front and forms an image out of axis in its focal plane. The measure of the image position in the first approximation gives directly the angle of the wave arrival for each space point where the lenslet is placed.

An attractive feature of this sensor is the simultaneous determination of the X and Y slopes by the measurement of the image position. The local slopes of the tested wave front $\psi(x,y)$ can therefore be detected from the relationships

$$\frac{\partial\psi(x,y)}{\partial x} = \frac{\Delta x}{F}, \quad \frac{\partial\psi(x,y)}{\partial y} = \frac{\Delta y}{F}, \quad (4.6)$$

where F is the focal length of the lenslets and Δx , Δy are the shifts of focus spots in the X- and Y-directions, respectively.

Usually, the Hartmann-Shack wave-front sensor requires the use of a reference plane wave, generated from a reference source in the instrument, in order to calibrate precisely the focus positions of the lenslet array. A number of methods can be used to measure the positions of the spots formed by the lenslets. The simplest technique is to use a quad-cell detector for each subaperture. But more precise results can be obtained using a CCD camera as a detector to record simultaneously all the images. An estimation of the spot position can be given in this case by the determination of its center-of-gravity:

$$\Delta x = \sum_{i,j} x_{ij} I_{ij} / \sum_{i,j} I_{ij}; \quad \Delta y = \sum_{i,j} y_{ij} I_{ij} / \sum_{i,j} I_{ij} \quad (4.7)$$

where I_{ij} and (x_{ij}, y_{ij}) are the signals and the positions of the pixel (i, j) , and the sum is made over all pixels of the subaperture devoted to a given lenslet.

Wave front reconstruction from the measured local slopes constitutes an inverse ill-posed problem and generally can be made by its orthogonal expansion [19]. Generally, the simplest method to solve it is based on the determination of pseudo-inverse matrix with the help of singular value decomposition procedure. We suppose to use the method for this purpose of optimal orthogonal expansion based on generalized eigen functions of forming operator [20].

B. Experimental setup

Fig. 4.11 shows an optical system developed to measure a Bragg cell distortion. The system consists of a He-Ne laser, ($\lambda=0.6328\mu$), collimators 1 and 2, beamsplitters 1 and 2, optical shutters, which permits to project objective and reference beams independently, CCD device with scaling video-system, which transform video-signals into 8-bit images of the size 684x512 pixels, and Hartmann- Shack wave front sensor HSS.

The microlens array is one of the most important elements of Hartmann-Shack wave-front sensor. We have developed a long-focal-length holographic lenslet array of 19×13 lenslets. The lenslets of the array have a focal length of 80mm and dimensions of 0.5 mm in diameter. The use of diffraction optics offers some advantages over the conventional refraction one: holographic lenslet arrays are easier to manufacture, less expensive, and can be produced with the variety of main parameters. Wave aberrations of holographic lenslet fall outside of the significant values ($\sim \lambda/20$ over the pupil 10×10 mm in the range of local wave slopes ± 20 minutes of arc, see below), and the chromatic aberrations are of no concern because of monochromatic laser light use. The average diameter of a formed spot in the focal plane was approximately $80 \mu\text{m}$ on the one-half intensity level. This matches well with the sizes of an

individual CCD cell ($\sim 9 \times 8.3 \mu\text{m}$), and no additional magnification was required.

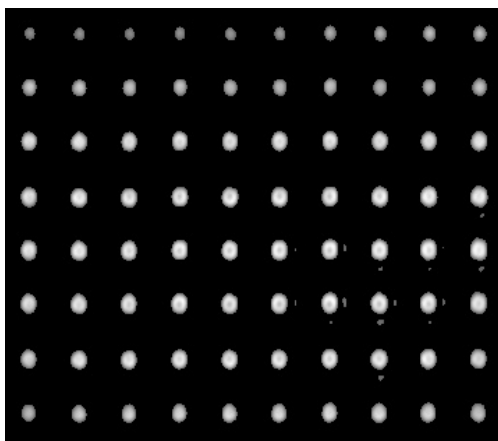


Fig. 4.12. A part of Hartmann-Shack image for a typical wave front

The system operates as follows: laser radiation is attenuated by polarizer attenuator to the proper level, and spatially filtered by collimator 1 with a pinhole in a focal point of reducing optics. Received plane wave is split on two beams by beamsplitter 1. The first wave illuminates wave front sensor and is used to form reference spots. The second wave is deflected by a Bragg cell being investigated, and, after proper reduction by a beam expander, forms an image frame in the plane of a CCD camera. The spatial filter PH blocks the 0-order of a Bragg cell. The shifts of the diffracted wave spot centers related to the reference beam are detected by CCD camera and processed by an image processor

using PC. Since the detected image in Hartmann-Shack sensor consists of only a number of focused spots, the signal-to-noise ratio in the image plane is high enough, and the sensitivity of the sensor is quite sufficient to satisfy the permissible exposure conditions.

A typical array of spot images is shown in Fig. 4.12. A small fluctuation in the peak intensity does not degrade the measurement accuracy in a treatment process that determines individual center positions of focal spots because only the energy centers are calculated.

C. Estimation of the centroid error of spots

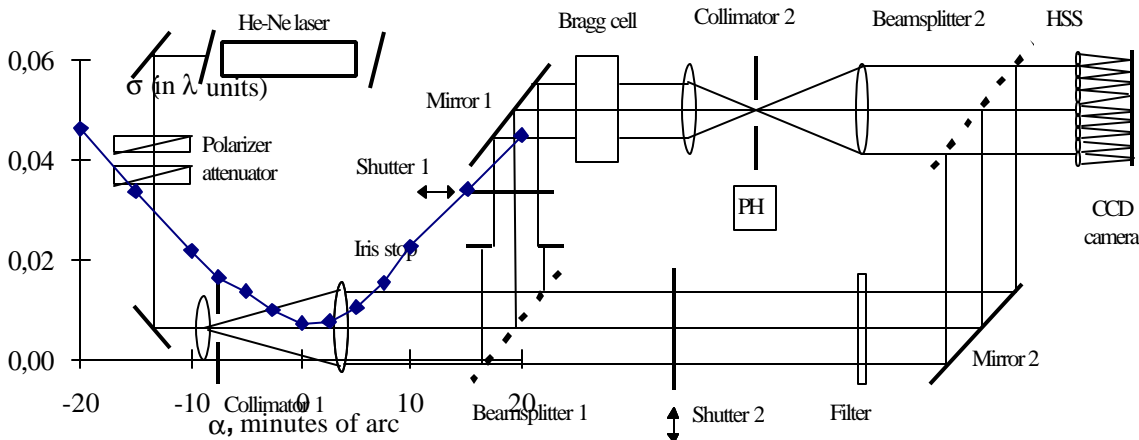


Fig. 4.13. Additional aberrations of inclined wave.

Fig. 4.11. Optical setup of Hartmann-Shack sensor.

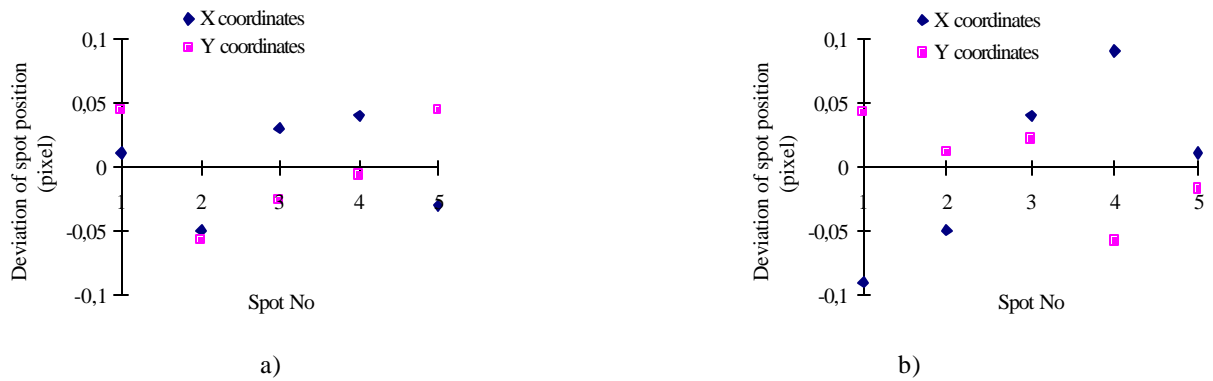


Fig. 4.14. Centroid unevenness for centered a) and peripheral b) spots

The centroid position of an image spot fluctuates from air turbulence, optics vibration, instability in laser intensity, and noise in CCD detector units. Because the centroid position relates directly to the local wave-front slope, the measurement accuracy is limited by the centroid errors. It is of great importance to estimate these errors and to reduce them as far as possible.

It should be noted that except random errors due to the factors pointed out above, the systematic errors can occur in estimated centroid positions as well. The main sources of systematic errors are the aberrations of diffraction lenslets, the misalignment of reference and object wave fronts, the inclination of a plane of a CCD camera detector, etc. In our experiments we estimated such errors in indirect way. To estimate the errors due to wave aberrations of holographic lenslets we use the plane wave-front precisely inclined to the plane of lenslet array. For aberration-free lenslets the estimated tilt has to be equal to the origin one, and the rms aberrations σ in excess over the pupil have to be vanishing. Fig. 4.13 shows the aberrations of inclined wave front measured in the range of ± 20 minutes of arc. One can see that wave aberrations due to holographic lenses do not exceed $\lambda/20$ (the total value of phase difference averaged over the pupil 10x10mm is $\sim 13\lambda$, thus the relative error comes to only 0.3% and is of no importance).

Random errors due to spot fluctuations were estimated by following procedure. Fig. 4.14 shows centroid fluctuations for five spot images among five-frame data without integration in the image processor. The standard

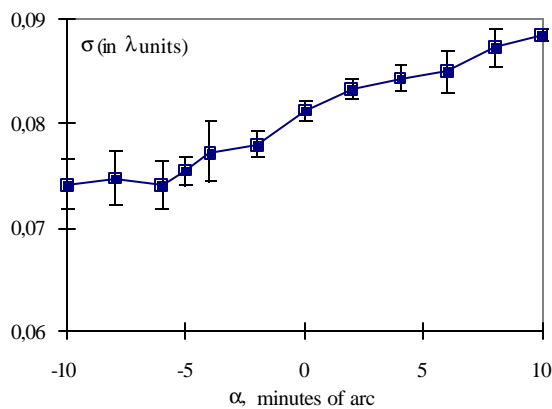


Fig. 4.15. Measured aberrations for wave front scanned by AO-deflector, α is tilt angle.

deviation of the spot center is about (in pixels) 0.039 in x -direction and 0.044 in y -direction for the spots in the center of a frame, and about 0.071(x) and 0.040(y) for the peripheral spots.

To calculate the corresponding error in a reconstructed wave front and reduce it, the data from a few spot frames of the same wave front were processed by inverse filtration, and the restored wave fronts (phase distributions over the pupil) were averaged. Then the standard deviation of the restored wave fronts from an averaged one was calculated, and it gave the estimation of a random error in the reconstructed wave front. Typical graph of measured average aberrations (plane wave scanned by a

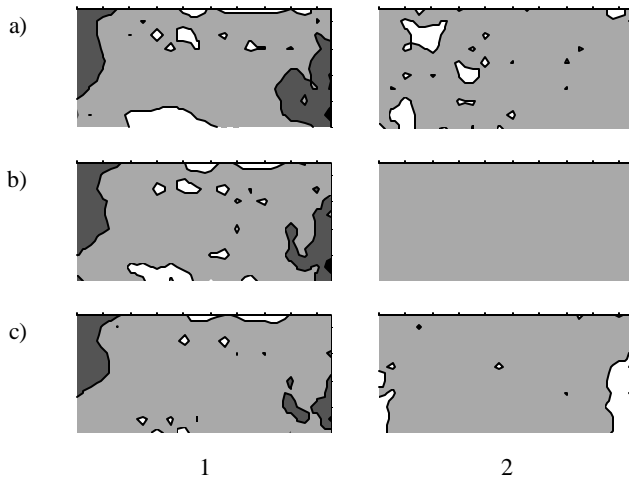


Fig. 4.16. The contour maps of wave aberrations of diffracted beam, 1)-with external reference beam, 2)-with reference beam at $f=100$ MHz; a)- $f=99$ MHz, b)- $f=100$ MHz, c)- $f=101$ MHz. All lines are plotted at $\lambda/10$ intervals. Real sizes are 5.5×2.5 mm

operating frequency of the analyzed frequency range falls normally on the lenslet array. This scheme permits to measure absolute aberrations of diffracted wave in relation to an incident light beam. The trouble is, that the reference and object wave fronts may be shifted in the plane of a lenslet array, and if the reference wave is not exactly plane, the additional artificial aberration may be registered.

The second group of experiments was performed using a diffracted wave on a central frequency as a reference beam. With this scheme, because the reference and the distorted beams pass through exactly the same optical path, optical aberrations in the measuring system are due to a Bragg cell distortions only. Therefore the aberrations of deflected wave front can be measured precisely, but yet these data are only relative, referring to the distorted diffracted wave front at 100 MHz.

The results obtained are shown in Fig. 4.16 where the contour phase maps are plotted over the performance aperture of exit pupil of a Bragg cell, in millimeters. Corresponding standard deviation of phase distortion as a frequency function are shown in Fig. 4.17. As might be expected from previous considerations, average phase distortion was appreciably higher for external reference beam, where uncontrollable phase errors may occur.

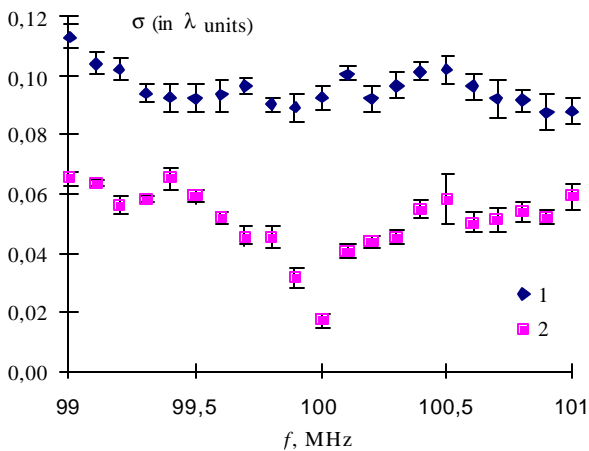


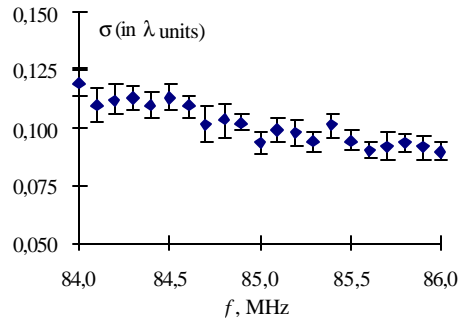
Fig. 4.17. Standard deviation of phase distortion in diffracted beam, 1)-with external reference beam, 2)- with reference beam at $f=100$ MHz

Bragg cell) with estimated rms errors are shown in Fig. 4.15. It is evident from the results that resulting random errors do not exceed $\sim \lambda/50$, that is comparable with the best devices of this type [21,22].

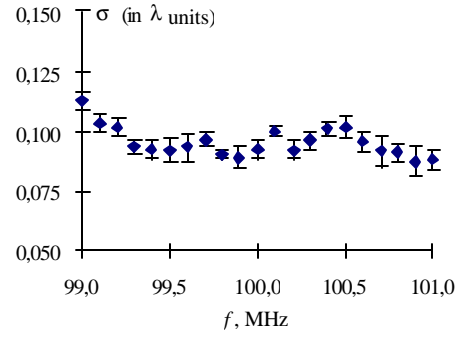
D. Experimental results and discussion

We have carried out two groups of experiments with especially fabricated Bragg cell on TeO_2 , which was designed in Section 3. In the first one, we have used a Bragg cell-input beam to produce the reference frame of the spots. The optical system is so adjusted that the reference wave front and tested wave front at the central

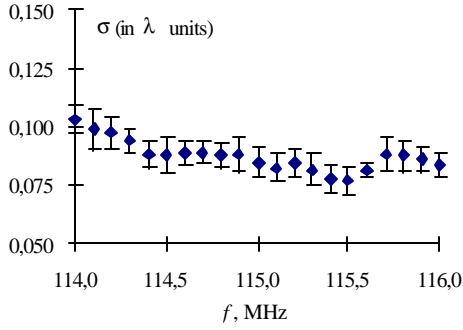
Because of data processing limitations, we were not able to register phase distribution over the whole wide frequency range simultaneously, therefore, we had performed measurements in three narrow frequency subranges. The results are shown in Fig. 4.18. We have not noticed the significant dependence of phase distortion on frequency. The only statement can be done with assurance that standard deviation of diffracted wave front varies within narrow (but detectable) limits with frequency variations. Nevertheless, detected phase distortions are in significant excess of systematic and random errors of the device, and hence, they are directly related with



a)



b)



c)

Fig. 4.18. Standard deviation of phase distortion in diffracted beam for three frequency subranges (reference beam is an input beam).

a)- $f=85\pm 1$ MHz; b)- $f=100\pm 1$ MHz; c)- $f=115\pm 1$ MHz.

irregularities in diffraction process. On the other hand, the absolute values of these distortions are rather small to not affect the output photocurrent phase. It means that carefully designing and fabricated a Bragg cell does not need any special reduction of spatial phase distortions.

Having no possibility to measure phase distribution of diffracted wave overall the operating range of a Bragg cell, we have performed research on phase distortions in the 0-order of diffraction (its wave front tilt does not change with frequency variance). It is well known, that 0- and 1-order modes in a Bragg cell are tightly coupled, hence, any phase variations in diffracted beam can cause some phase change in non-diffracted wave. The results are shown in Fig. 4.19. As the reference beam was taken the direct wave passing the Bragg cell with no sound intensity.

It can be said with assurance that variations in phase map with frequency variation is directly coupled with frequency response (FR) of the Bragg cell. The corresponding FR is presented in Fig. 4.20 and displays an 0-order intensity dependence on frequency and, hence, corresponding phase variations in 1-order diffraction. As it is evident, these variations are well-correlated: the maximum standard deviation of phase distortion corresponds to limits of FR, as exemplified by the graphs of FR and standard deviation of phase distortion in the 0-order. It is essential to conduct further investigations to make more detail conclusions of physical and technical significance of this effect.

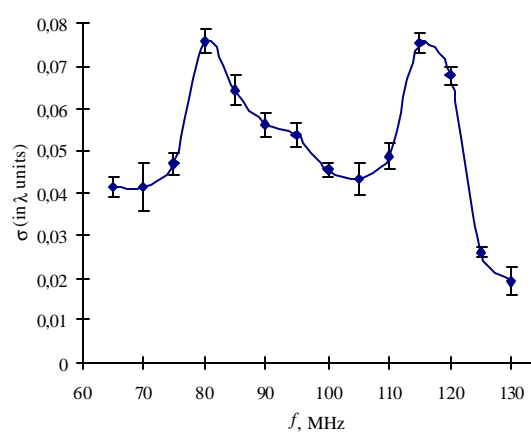
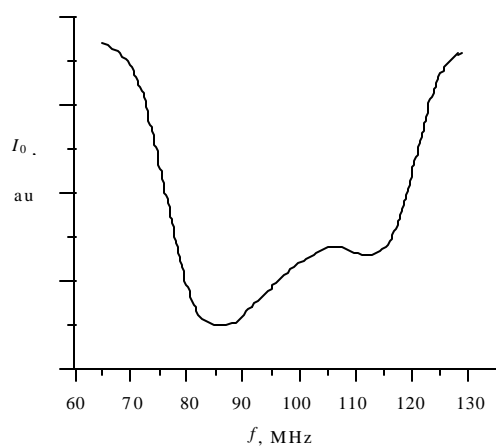
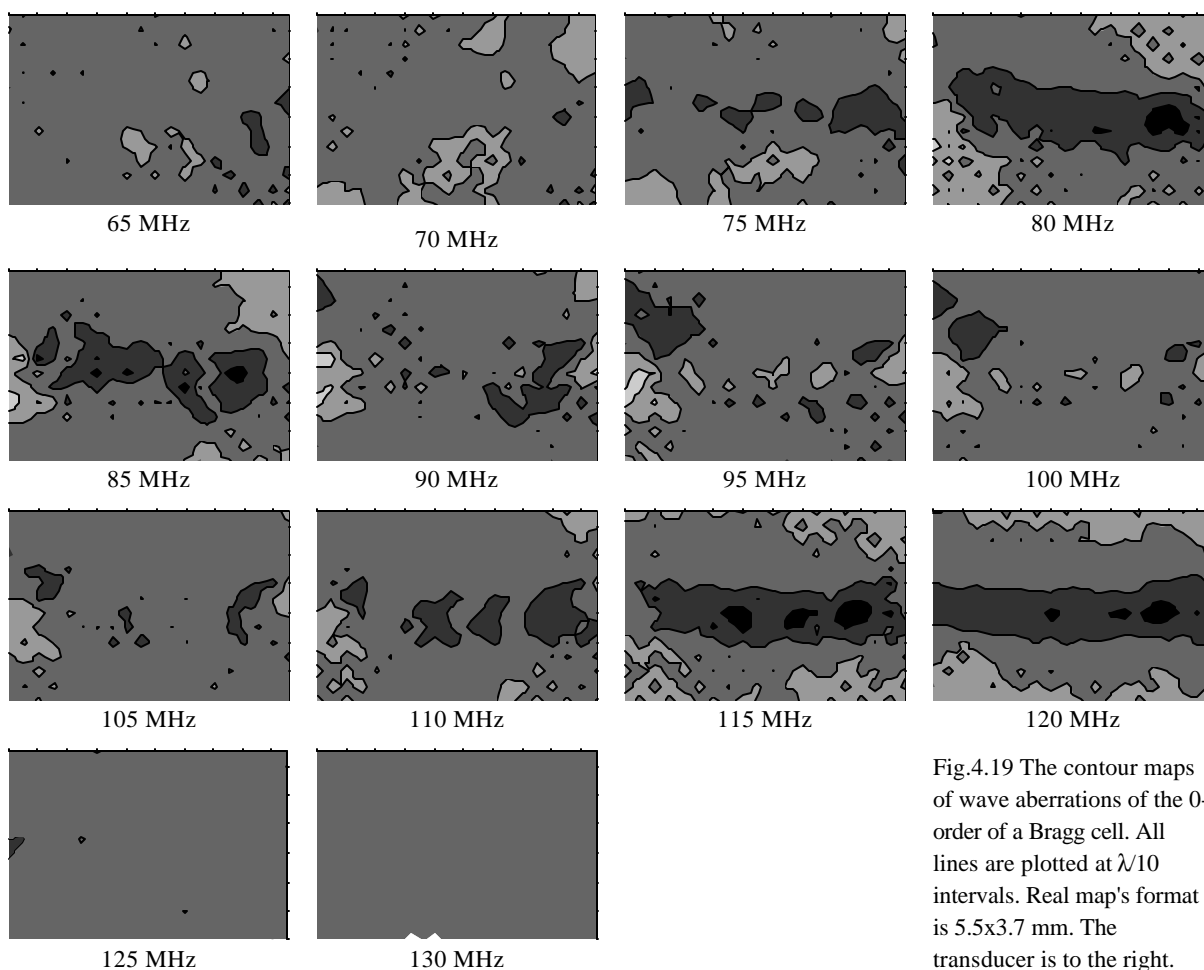


Fig. 4.20. Frequency response function of a Bragg cell (a), and standard deviation of phase distortion in the 0-order (b).

5. Conclusion

Phase characteristics of a Bragg cell in an optical coherent signal processing system are investigated. In Section 1, a conversion of signals by a Bragg cell is considered, and a definition of its phase response (PhR) as an equivalent opto-electronic quadripole characteristic is introduced.

In Section 2, an influence of a Bragg cell on an output phase of a heterodyne optical system is investigated using a numerical simulation. It is stated that a Gaussian beam truncation by a Bragg cell and sound decay does not practically affect an output photocurrent phase if there are no irregular perturbations of diffracted wave-front. Such perturbations can be caused, for example, by a Bragg cell optical non-homogeneity, technological errors during its fabrication, or thermal effects. In this case an output phase will depend on as irregularity types as a photodetector size. Especially, phase distortions become appreciable when that size makes a part of a light spot size. That may be important in case when a diode array is used, and reference probes are narrower than a signal mainlobe. When the photodetector size is greater than a spot one, an averaging occurs and output phase distortions decreases to zero. Thus in practice, a Bragg cell influence has to be appreciable only in a system with a number of photodetectors per spot ≥ 2 .

Criteria to design a Bragg cell with small phase distortions are formulated in Section 3. A principle used as a basis is to minimize an absorbed acoustic power since it causes thermal distortions. A connection has been analyzed of the proposed criterion with basic Bragg cell parameters: an aperture, efficiency, resolution. A Bragg cell on TeO_2 for light wavelength $0.633 \mu\text{m}$ with operating frequency 100 MHz (bandwidth ~ 30 MHz) and efficiency 0.9 has been designed. A design example of a GaAs Bragg cell for light wavelength $1.55 \mu\text{m}$ with the same operating frequency is presented. It is shown that it can be more effectively used in a much higher frequency range.

In Section 4 experimental investigations are carried out of a specially fabricated Bragg cell on TeO_2 designed in Section 3. The fabricated Bragg cell had the bandwidth 81.7-114.2 MHz on the minimum efficiency level of 0.86 with non-uniformity of 4% (above the efficiency 0.86) at the input electrical power equal to 130 mw. Its input VSWR was less than 2.55 within the bandwidth.

Its phase characteristics in an optical heterodyne system have been measured. It is shown that conventional approach based on the use of a Mach-Zehnder interferometer and a RF phase meter is not suitable to measure phase response in an overall frequency range because of its steep slope. A new two-frequency technique is proposed to make such measurements. The idea is to use two signals with slightly different frequencies simultaneously, and to measure a phase of a difference frequency signal extracted from the photodetector output. In the experiment there was used a frequency difference equal to 50 kHz. The photodetector size was much larger than a focused light spot.

Using this technique, phase response were measured within the range of 75-125 MHz at different input powers (from 10 to 100 mw). There was found no dependence of phase response on power but its considerable nonlinearity was discovered, and correspondingly, essential dependence of delay time on frequency was found. It is shown that observed dependence is connected with used approach to define and measure a phase response as “the inserted phase response” of an equivalent quadripole. In this case, the output phase is measured relative to a phase of a Bragg cell input signal which is considered as a reference. Therefore a measured phase difference becomes dependent on a Bragg cell input impedance. If this dependence has excluded, then the dependence of output phase on frequency is disappeared as well. What that means for practice one could conclude only considering a concrete Bragg cell application in an opto-electronic system. Thus, in a certain sense, one can say the experiment confirmed

that in a heterodyne system a Bragg cell does not practically distort a phase response if the photodetector size is much larger than a light spot.

Also in Section 4 wave-front distortions of a Bragg cell were measured as in the first as in the zero order using a Hartmann-Shack sensor. The estimated accuracy of measurement was not worse than $\lambda/50$. Distortions within three narrow subranges (84-86, 99-101, 114-116 MHz) had been measured in the 1st diffraction order. There was found no dependence of wave-front distortions on frequency within the overall range. Nevertheless, detected phase distortions within subranges are in significant excess of systematic and random errors (they are in the order of $\lambda/40$), so that they are apparently connected with irregularities in diffraction process. Their absolute values are rather small to not affect an output photocurrent phase in heterodyne system in common case. At the same time, measurements in the zero order show that in overall operating range there are appreciable distortions (in the order of $\lambda/25$), which can be possibly observed in the 1st order too. They can certainly to affect an output phase if a photodetector size is less than a light spot. In this case one can expect that an unavoidable frequency dependent phase noise will arise in the output causing a dynamic range reduction.

It should be also noted, that in testing optical systems, wave-front distortions inserted by a Bragg cell can significantly deteriorate their parameters.

Thus, the basic results of the work are as follows:

1. A Bragg cell in a heterodyne (coherent) signal processing system does not insert any appreciable phase distortions into an output signal unless a photodetector size is less than a light spot one.
2. Otherwise, such distortions can offer and be appreciable causing an unavoidable frequency dependent phase noise and a dynamic range reduction.
3. In testing optical systems a Bragg cell wave-front distortions can cause a deterioration of system parameters.

From the aforesaid follows that further experimental investigations using a photodiode array are useful and necessary to learn vividly real limitations of considered opto-electronic system application.

Obtained results have been partly presented at the ICA/ASA '98 meeting, (Seattle, USA, June 20-26, 98), and also have been accepted for presentation at the 8th International Crimea Microwave Conference CriMiCo'98 (Sevastopol, Ukraine, 14-17 Sept.), and at the International Conference "Optical Storage" - OS'98 (Kiev, Ukraine, 28 Sept.-2 Oct.).

References

Acousto-optic signal processing. Theory and implementation. /Edited by N.J. Berg, J.M. Pellegrino. Marcel Dekker, Inc., NY, 1996.

V.V. Protopopov, N.D. Ustinov. Laser heterodyning. - Moscow: Nauka, 1985. (in Russian)

V.V. Kludzin. Peculiarities of optical heterodyning in acousto-optic devices. Optics & Spectroscopy, (in Russian).

O.B. Gusev, S.V. Kulakov, B.P. Razzhivin, D.V. Tigin. Optical signal processing in real time. - Moscow: Radio i svyaz, 1989, (in Russian).

"The Study of the Phase Characteristics of Bragg Cells for Acousto-Optic Signal Processing". The first stage report on the special contract of EOARD SPC-97-4025. Kiev Taras Shevchenko University, 1997.

- R. McLeod, K. Wu, K. Wagner, R. Weverka. Acousto-optic photonic crossbar switch. Part 1: design. Appl. Opt., v. 35, #32, 6331-6353, 1996.
- V.A. Goncharov, L.N. Ilchenko, V.M. Moskalev, E.N. Smirnov, A.V. Yurchenko. Visualization of a Phase Structure of Sound Field in a Bragg Cell. Proceedings of the ICA/ASA '98 meeting. 20-26 June 1998, Seattle, Washington.
- L.N. Magdich, V.Ya. Molchanov. Acoustooptic devices and their applications. New York: Gordon and Breach Science Publishers, 1989.
- A.V. Yurchenko, Yu.L. Oboznenko, V.M. Moskalev, D.M. Stevens. Bragg Cell on TeO_2 for 2-D Deflector with Reduced Drive Power - Analysis, Design, and Experimental Examination. Wright Laboratory Technical Report # WL-TR-1997-1192 (DTIC), 1997. National Technical Information Service <http://www.ntis.gov/>
- R.W. Dixon. Photoelastic properties of selected materials and their relevance for applications of acoustic light modulators and scanners. J. Appl. Phys., v.38., #13, p. 5149-5153.
- Balakshiy V.I., Parygin V.N., Chirkov L.E. Physical foundation of acoustooptics.- Moscow: Radio i svyaz, 1985, (in Russian).
- J.F. Nye. Physical properties of crystals. Their representation by tensors and matrices. Oxford at the Clarendon Press, 1957.
- Acoustic crystals. Handbook. - Ed. Shaskol'skaya M.P. - Moscow: Nauka, 1982, (in Russian).
- R.W. Damon, W.T. Maloney, D.H. McMahon. Light - ultrasound interaction. Ch. 5 in the book Physical Acoustics. Principles and Methods. /Edited by W.P. Mason, v. VII (Russian translation) Moscow: Mir, 1974.
- A. Korpel. Acousto-optics. Marcel Dekker, Inc. New York and Basel, 1988.
- J.R. Finup. Phase retrieval algorithms: a comparison. Appl. Opt., v. 21, No. 15, 2758-2769, 1982.
- R.W. Gerchbery, W.O. Saxton. A practical algorithm for the determination of phase from image and diffraction plane pictures. Optik, v. 35, No. 2, p.237-246, 1972;
- R. A. Gonsalves J. Opt. Soc. Am., **66**, p.961, 1976.
- R. Shack and B. Platt. Optical Science Newsletter, Univ. Of Arizona, Tucson, Ariz., **5**, N1, p.15, 1971.
- Adaptive Optics for Astronomy*, Ed. D. M. Alloin and J.-M. Mariotti, NATO ASI Series: C; **423**, Kluwer Academic Publ., 1994.
- V. V. Molebny, V. N. Kurashov, D. V. Podanchuk, A. V. Kovalenko I. G. Pallikaris, L. P. Naoumidis, Proc. SPIE, **3246**, p.328 1998.
- G. Y. Yoon, T. Jitsuno, M. Nakatsuka, and S. Nakai. Appl Opt., **35**, p.188, 1996.
- H. Hamam. Appl Opt., **37**, p.1393, 1998.